

Article

Static and Dynamic Response of FG-CNT-Reinforced Rhombic Laminates

Md Irfan Ansari ¹ , Ajay Kumar ^{1,*} , Danuta Barnat-Hunek ², Zbigniew Suchorab ^{3,*}, Wojciech Andrzejuk ⁴ and Dariusz Majerek ⁵

¹ Department of Civil Engineering, National Institute of Technology Patna, Patna-800005, India; er.mdirfan2k9@gmail.com

² Faculty of Civil Engineering and Architecture, Lublin University of Technology, Nadbystrzycka St. 40, 20-618 Lublin, Poland; d.barnat-hunek@pollub.pl

³ Faculty of Environmental Engineering, Lublin University of Technology, Nadbystrzycka St. 40B, 20-618 Lublin, Poland

⁴ Faculty of Economics and Engineering, Pope John Paul II State School of Higher Education in Białystok, Sidorska St. 95/97, 21-500 Białystok, Poland; w.andrzejuk@dydaktyka.pswbp.pl

⁵ Faculty of Fundamentals of Technology, Lublin University of Technology, Nadbystrzycka St. 38, 20-618 Lublin, Poland; d.majerek@pollub.pl

* Correspondence: sajayedce@gmail.com (A.K.); z.suchorab@pollub.pl (Z.S.); Tel.: +91-612-2371929 (A.K.); +48-81-5384322 (Z.S.)

Received: 30 March 2018; Accepted: 30 April 2018; Published: 21 May 2018



Abstract: The present study focuses on the static and dynamic response of functionally graded carbon nanotube (FG-CNT)-reinforced rhombic laminates. The cubic variation of thickness coordinate in the displacement field is considered in terms of Taylor's series expansion, which represents the higher-order transverse cross-sectional deformation modes. The condition of zero-transverse shear strain at upper and lower surface of FG-CNT-reinforced rhombic laminates is imposed in the present formulation. The present two-dimensional model is formulated in a finite element, with the C⁰ element consisting of seven nodal unknowns per node. The final material properties of FG-CNT-reinforced rhombic laminates are estimated using the rule of mixture. The obtained numerical results are compared with the results available in the literature to verify the reliability of the present model. The present study investigates the effect of CNT distribution, loading pattern, volume fraction, and various combinations of boundary constraints by developing a finite element code in FORTRAN.

Keywords: plates; carbon nanotubes; structure; skew; finite element method; deflection; frequency

1. Introduction

Recently, composite plates reinforced by carbon nanotubes (CNTs) have gained significant attention in civil, aeronautical, mechanical, and marine engineering due to their high strength/weight ratio and low density. The CNTs discovered by Iijima [1] are made up of the molecular-scale tube-like structure of carbon allotropes having fine materialistic properties. The CNTs are generally used in composites to improve their elastomechanical and thermal properties by dispersing in the matrix [2,3]. Various plate theories have been developed by the researchers to analyze the plates. The classical plate theory (CPT) model is based on the Kirchhoff–Love hypothesis that straight lines remain straight and perpendicular to the midplane after deformation. The transverse shear stress components are neglected in the CPT, where it is included in the shear deformation theory by Reissner [4]. In Reissner's shear deformation theory, a shear correction factor is required for strain equations. Zhu et al. [5] discussed the effect of single-walled CNTs on the bending and vibration analysis of a CNT-reinforced

composite (CNTRC) plate using first-order shear deformation theory (FSDT). They used the rule of the mixture to calculate the final material properties of CNTRC plate. The free vibration analysis of uniaxially aligned single-walled carbon nanotubes (SWCNTs)-reinforced composite was conducted by Lei et al. [6] by incorporating FSDT along with element-free kp-Ritz method. The static analysis of CNTRC cylinders using the mesh-free method was studied by Dastjerdi et al. [7]. Yas et al. [8] developed a three-dimensional solution for free vibration analysis of SWCNTs-reinforced composite cylindrical panel. The differential quadrature method and FSDT-based governing equation were used by Malekzadeh and Zarei [9] to examine the free vibration behavior of FG-CNT-reinforced laminated plate. The free vibration analysis of FG-CNTRC plate was presented by Nami and Janghorban [10] using the differential quadrature method. Shahrbabaki and Alibeigloo [11] used the Ritz method for the three-dimensional vibration analysis of CNTRC plate. They have calculated the effective material properties of the reinforced composite using the modified rule of mixture. Sankar et al. [12] used HSDT to study the static and free vibrations of FG-CNTRC plates and sandwich plates. The effect of uniform thermal environment on FG-CNTRC plate was studied by Mehar et al. [13] while the effect of non-uniform thermal load on FG-CNTRC beam was analyzed by Mayandi and Jeyaraj [14] using the finite element method. Zhang et al. [15] incorporated FSDT along with the element-free Ritz method to analyze a CNTRC plate with elastically restrained edges. Huang et al. [16] discussed the vibration and bending behavior of antisymmetric laminated functionally graded CNT-reinforced plate using FSDT containing four variables. Macias et al. [17] used FSDT for the static and free vibration analysis of FG-CNTRC skew plate using a four-noded shell element. Mirzaei and Kiani [18] used FSDT and Song et al. [19] considered HSDT for the vibration analysis of functionally graded CNTRC cylindrical panels and the ultimate properties of the composite were calculated by the refined rule of mixture. Thomas and Roy [20] studied the influence of UD-CNT and FG-CNT on the vibration of different type of shell structures reinforced by CNTs. The advanced fabrication and properties of aligned carbon nanotube composites were explained by Duong et al. [21]. Both Selim et al. [22] and Zhang and Selim [23] used a Reddy's higher order shear deformable model for the vibration analysis of FG-CNTRC plate using the mesh-free method. Manevitch et al. [24] explored the nonlinear optical vibration behavior of SWCNTs. Fantuzzi et al. [25] studied the free vibration analysis of an arbitrarily shaped FG-CNT-reinforced plate using NURBS curves. The effect of agglomerated CNT on the linear static analysis of nanocomposite plate and shell was studied by Tornabene et al. [26]. Size phenomena in elastic nanobeams can be conveniently carried out by stress-driven nonlocal continuum mechanics proposed by Romano and Barretta [27] to overcome all difficulties of the strain-driven nonlocal theory of elasticity. A general treatment on nonlocal integral formulations of elasticity for nanomaterials is presented in [28] and successfully applied by [29–32] to size-dependent static and dynamic structural problems of current technical interest. Ansari et al. [33] provided a numerical solution for the vibration analysis of FG-CNTRC elliptical plates and the extended rule of the mixture was used for calculating the effective material properties. The free vibration analysis of nanocomposite plate and shell using FSDT was explored by Tornabene et al. [34]. Ardestani et al. [35] discussed the effect of orientation of CNT on the static and vibration behavior of FG-CNTRC skew plates.

The literature review indicates that few works for the static and dynamic analysis of FG-CNT-reinforced rhombic laminates are available. Therefore, in this paper, an effort was made to conduct a behavioral study of the FG-CNT rhombic laminates using HSDT, which removes the need for a shear correction factor. The finite element coding was developed by authors of the present mathematical model using a C^0 nine-noded finite element. Since results for FG-CNT-reinforced rhombic laminates subjected to trigonometrical loading are not available in the literature, the present analysis results may serve as a benchmark for the researchers working in this field.

2. Carbon Nanotube-Reinforced Laminates

Figure 1 depicts the geometry of the FG-CNT-reinforced plate used in the present study. The length and width of the plate are taken as a and b with the total thickness h . The middle section was taken

as a reference for the material coordinates (x , y , z) of the rhombic plate. Four types of distribution were considered, as adopted by Zhu et al. [5], namely UD, FG-O, FG-X and FG-V of CNTs inside a polymer matrix within CNT-reinforced composite plate in the thickness direction. The ultimate material properties of the FG-CNT-reinforced rhombic plate were determined in accordance with the rule of mixture [36,37].

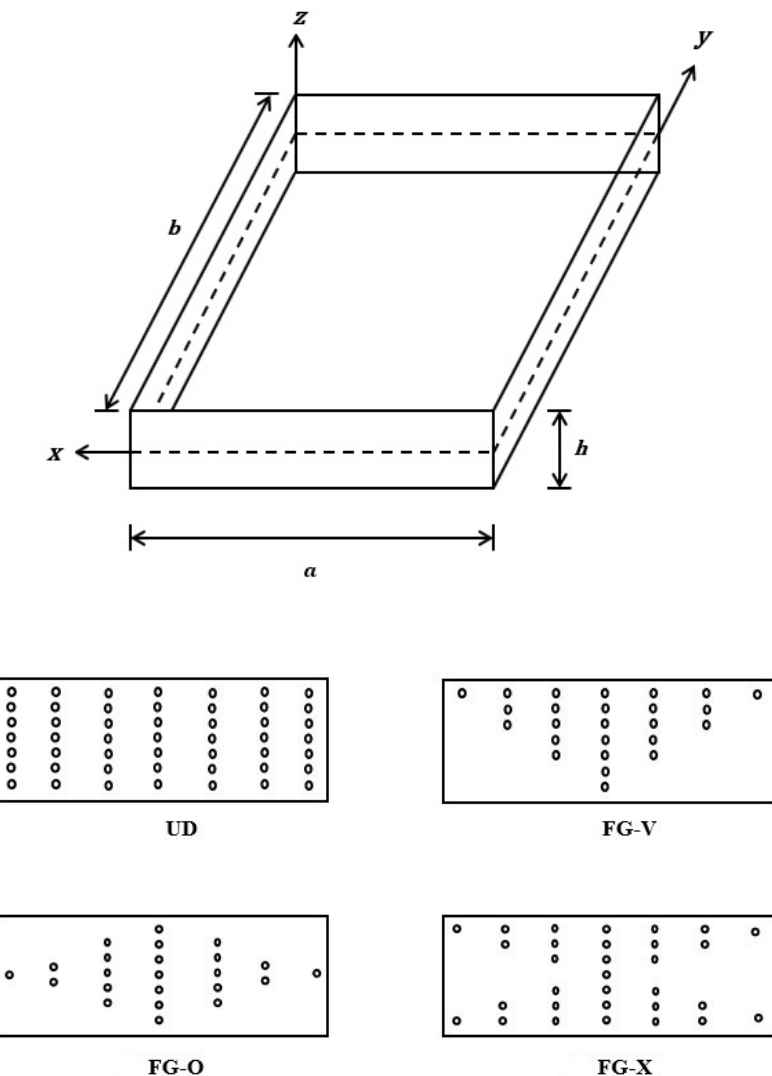


Figure 1. The geometry and configuration of carbon nanotube reinforced plate.

The volume fraction of uniform distribution and functionally graded distributions of the CNTs along the thickness direction of the CNT-reinforced rhombic plates shown in Figure 1 was assumed to be as follows:

$$V_{\text{CNT}}(z) = \begin{cases} V_{\text{CNT}}^* & (\text{UD}) \\ 2\left(1 - \frac{2|z|}{h}\right)V_{\text{CNT}}^* & (\text{FG-O}) \\ 2\left(\frac{|z|}{h}\right)V_{\text{CNT}}^* & (\text{FG-X}) \\ \left(1 + \frac{2z}{h}\right)V_{\text{CNT}}^* & (\text{FG-V}) \end{cases} \quad (1)$$

where $V_{\text{CNT}}^* = \frac{w_{\text{CNT}}}{w_{\text{CNT}} + (\rho^{\text{m}}/\rho^{\text{m}}) - (\rho^{\text{CNT}}/\rho^{\text{m}})w_{\text{CNT}}}$,

where w_{CNT} is the mass fraction of the CNTs in the CNT-reinforced rhombic plates, whereas ρ^{m} and ρ^{CNT} are the densities of the polymer matrix and carbon nanotubes, respectively.

In line with the rule of mixture, the effective material properties of FG-CNT-reinforced plates were employed by introducing the CNT efficiency parameters; thus, the final properties can be written as follows [38]:

$$E_{11} = \eta_1 V_{\text{CNT}} E_{11}^{\text{CNT}} + V_m E^m \quad (2)$$

$$\frac{\eta_2}{E_{22}} = \frac{V_{\text{CNT}}}{E_{22}^{\text{CNT}}} + \frac{V_m}{E^m} \quad (3)$$

$$\frac{\eta_3}{G_{12}} = \frac{V_{\text{CNT}}}{G_{12}^{\text{CNT}}} + \frac{V_m}{G^m} \quad (4)$$

$$\nu_{12} = V_{\text{CNT}}^* \nu_{12}^{\text{CNT}} + V_m \nu^m \quad (5)$$

$$\rho_{12} = V_{\text{CNT}}^* \rho_{12}^{\text{CNT}} + V_m \rho^m, \quad (6)$$

where E_{11}^{CNT} and E_{22}^{CNT} are Young's moduli and G_{12}^{CNT} is the shear modulus of singly walled CNTs, respectively. E^m and G^m are known as Young's modulus and shear modulus of the isotropic matrix. ν_{12}^{CNT} and ν^m represent the Poisson's ratio of CNTs and matrix respectively. V_m and V_{CNT} are the volume fractions of the matrix and carbon nanotubes, respectively, and the sum of both volume fractions equals to unity. η_1 , η_2 , η_3 are the scale-dependent material properties and they can be calculated by matching the effective properties of CNT-reinforced composite obtained from the MD simulations with those from the rule of mixture.

3. Mathematical Formulation

3.1. Displacement Fields and Strains

The displacement field for the FG-CNT-reinforced rhombic plate is considered to derive the mathematical model based on the third-order shear deformation theory [39]:

$$\begin{aligned} u(x, y, z) &= u_0(x, y) + z\theta_x(x, y) + z^2\xi_x(x, y) + z^3\zeta_x(x, y) \\ v(x, y, z) &= v_0(x, y) + z\theta_y(x, y) + z^2\xi_y(x, y) + z^3\zeta_y(x, y) \\ w(x, y, z) &= w_0(x, y) \end{aligned}, \quad (7)$$

where u , v and w are the displacements of any generic point in the plate geometry, (u_0 , v_0 and w_0) are displacements at the mid-plane and θ_x , θ_y are the bending rotations defined at the midplane about the y and x -axes respectively. ξ_x , ξ_y , ζ_x and ζ_y are higher order terms of Taylor's series expansion. The function ξ_x , ξ_y , ζ_x and ζ_y will be calculated by vanishing shear stress at top and bottom of the plate. By applying the boundary conditions $\gamma_{xz}(x, y, \pm h/2) = \gamma_{yz}(x, y, \pm h/2) = 0$ at the upper layer and lower layer of the plate in Equation (7) and rearranging the terms that appear in the displacement field (u and v), we obtained

$$\xi_x = \xi_y = 0 \quad (8)$$

$$\zeta_x = -\frac{4}{3h^2} \left(\theta_x + \frac{\partial w}{\partial x} \right), \quad \zeta_y = -\frac{4}{3h^2} \left(\theta_y + \frac{\partial w}{\partial y} \right). \quad (9)$$

By substituting Equations (8) and (9) into Equation (7), we obtain

$$\begin{aligned} u(x, y, z) &= u_0 + \left(z - \frac{4z^3}{3h^2} \right) \theta_x - \frac{4z^3}{3h^2} \left(\frac{\partial w}{\partial x} \right) \\ v(x, y, z) &= v_0 + \left(z - \frac{4z^3}{3h^2} \right) \theta_y - \frac{4z^3}{3h^2} \left(\frac{\partial w}{\partial y} \right) \\ w(x, y, z) &= w_0 \end{aligned}. \quad (10)$$

If the displacement field represented in Equation (10) is implemented in the strain part, the problem of C^1 continuity requirement in the higher-order theory may arise due to the existence of

first-order derivatives of transverse displacement. By applying C^0 continuity to the present problem, the out of plane derivatives are exchanged by the following relations in Equation (10):

$$\psi_x = \frac{\partial w}{\partial x}, \quad \psi_y = \frac{\partial w}{\partial y}. \quad (11)$$

The final form of higher order theory possessing C^0 continuity may be presented in the following manner:

$$\begin{aligned} u(x, y, z) &= u_0 + \left(z - \frac{4z^3}{3h^2} \right) \theta_x - \frac{4z^3}{3h^2} \psi_x \\ v(x, y, z) &= v_0 + \left(z - \frac{4z^3}{3h^2} \right) \theta_y - \frac{4z^3}{3h^2} \psi_y \\ w(x, y, z) &= w_0 \end{aligned} \quad (12)$$

Hence, the basic field variables interpreted in the present investigation with the assumption of constant transverse displacement component are u_0 , v_0 , w_0 , θ_x , θ_y , ψ_x , and ψ_y for each node. Mathematically, the nodal displacement vector $\{\delta\}$ corresponding to displacement field in Equation (12) may be represented as

$$\{\delta\} = [u_0 \ v_0 \ w_0 \ \theta_x \ \theta_y \ \psi_x \ \psi_y]^T \quad (13)$$

From the displacement field presented above in Equation (12), the strain can be written as

$$\{\varepsilon\} = \{\varepsilon_x, \varepsilon_y, \gamma_{xy}, \gamma_{xz}, \gamma_{yz}\}^T. \quad (14)$$

Furthermore, the expression of strain vector $\{\varepsilon\}$ can be correlated with the displacement vector $\{\delta\}$ by means of the following relationship:

$$\{\varepsilon\} = [B]\{\delta\}, \quad (15)$$

where $[B]$ is known as a strain-displacement matrix and involves the derivatives of shape function terms. Since the plane stress problem is considered in the analysis, the components of strain vector may be represented as

$$\begin{aligned} \varepsilon_x &= \frac{\partial u}{\partial x} \\ \varepsilon_y &= \frac{\partial v}{\partial y} \\ \gamma_{xy} &= \frac{\partial u}{\partial y} + \frac{\partial v}{\partial x} \\ \gamma_{xz} &= \frac{\partial u}{\partial z} + \frac{\partial w}{\partial x} \\ \gamma_{yz} &= \frac{\partial v}{\partial z} + \frac{\partial w}{\partial y}. \end{aligned} \quad (16)$$

The strain relationships can be written as

$$\begin{aligned} \varepsilon_x &= \varepsilon_{x0} + z \left(1 - \frac{4z^2}{3h^2} \right) k_x - \frac{4z^3}{3h^2} k_x^* \\ \varepsilon_y &= \varepsilon_{y0} + z \left(1 - \frac{4z^2}{3h^2} \right) k_y - \frac{4z^3}{3h^2} k_y^* \\ \gamma_{xy} &= \gamma_{xy0} + z \left(1 - \frac{4z^2}{3h^2} \right) k_{xy} + \frac{4z^3}{3h^2} k_{xy}^* \\ \gamma_{xz} &= \phi_x - \frac{4z^2}{h^2} k_{xz} - \frac{4z^2}{3h^2} k_{xz}^* \\ \gamma_{yz} &= \phi_y - \frac{4z^2}{h^2} k_{yz} - \frac{4z^2}{3h^2} k_{yz}^*, \end{aligned} \quad (17)$$

where

$$\begin{aligned}\varepsilon_{x0} &= \frac{\partial u_0}{\partial x}, \quad \varepsilon_{y0} = \frac{\partial v_0}{\partial y}, \quad \gamma_{xy0} = \frac{\partial u_0}{\partial y} + \frac{\partial v_0}{\partial x} \\ \phi_x &= \frac{\partial w_0}{\partial x} + \theta_x, \quad \phi_y = \frac{\partial w_0}{\partial y} + \theta_y \\ k_x &= \frac{\partial \theta_x}{\partial x}, \quad k_y = \frac{\partial \theta_y}{\partial y}, \quad k_{xy} = \frac{\partial \theta_x}{\partial y} + \frac{\partial \theta_y}{\partial x}, \quad k_{xz} = \theta_x, \quad k_{yz} = \theta_y \\ k_x^* &= \frac{\partial \psi_x}{\partial x}, \quad k_y^* = \frac{\partial \psi_y}{\partial y}, \quad k_{xy}^* = \frac{\partial \psi_x}{\partial y} + \frac{\partial \psi_y}{\partial x}, \quad k_{xz}^* = \psi_x, \quad k_{yz}^* = \psi_y.\end{aligned}$$

3.2. Constitutive Relationship

The stress-strain relationship for the CNTRC rhombic plate can be written as

$$\{\sigma\} = [Q]\{\varepsilon\}, \quad (18)$$

where the constitutive matrix is

$$[Q] = \begin{bmatrix} Q_{11} & Q_{12} & 0 & 0 & 0 \\ Q_{21} & Q_{22} & 0 & 0 & 0 \\ 0 & 0 & Q_{33} & 0 & 0 \\ 0 & 0 & 0 & Q_{44} & 0 \\ 0 & 0 & 0 & 0 & Q_{55} \end{bmatrix}, \quad (19)$$

$$\text{where } Q_{11} = \frac{E_{11}}{1 - \nu_{12}\nu_{21}}, \quad Q_{22} = \frac{E_{22}}{1 - \nu_{12}\nu_{21}}, \quad Q_{12} = \frac{\nu_{21}E_{11}}{1 - \nu_{12}\nu_{21}}, \quad Q_{33} = Q_{44} = Q_{55} = G_{12}. \quad (20)$$

4. Finite Element Formulation

4.1. Element Description

A nine-node C^0 isoparametric Lagrangian element was utilized in the present investigation. The element has a total of 63 degrees of freedom and each node has seven degrees of freedom. The element has inconsistent rectangular geometry in the x–y coordinate system. In order to ensure a consistent rectangular geometry, the element was plotted to the ξ – η plane. For the assumed nine-node element, the expressions for shape functions N_i are described below.

For corner nodes:

$$N_1 = \frac{1}{4}(\xi - 1)(\eta - 1)\xi\eta, \quad N_3 = \frac{1}{4}(\xi + 1)(\eta - 1)\xi\eta, \quad N_7 = \frac{1}{4}(\xi - 1)(\eta + 1)\xi\eta, \quad N_9 = \frac{1}{4}(\xi + 1)(\eta + 1)\xi\eta. \quad (21)$$

For middle nodes:

$$N_2 = \frac{1}{2}(1 - \xi^2)(\eta^2 - \eta), \quad N_4 = \frac{1}{2}(\xi^2 - \xi)(1 - \eta^2), \quad N_6 = \frac{1}{2}(\xi^2 + \xi)(1 - \eta^2), \quad N_8 = \frac{1}{2}(1 - \xi^2)(\eta^2 + \eta). \quad (22)$$

For the center node:

$$N_5 = (1 - \xi^2)(1 - \eta^2). \quad (23)$$

4.2. Governing Equation for Bending Analysis

The expression of strain energy may be given as

$$\delta U = \iiint \{\delta\varepsilon\}^T \{\sigma\} dx dy dz. \quad (24)$$

By utilizing the relationship of Equation (18), the above equation can be written as

$$\delta U = \iint \{\delta \varepsilon\}^T [D] \{\varepsilon\} dx dy \quad (25)$$

where $[D] = \int [H]^T [Q] [H] dz$,

where $[H]$ is the matrix that contains the terms involving z and h .

The change in strain vector may be written as $\{\delta \varepsilon\} = [B] \{\delta X\}$.

By using Equations (15) and (25), the stiffness matrix $[K]$ can be written in the following form:

$$[K] = \iint [B]^T [D] [B] dx dy. \quad (26)$$

4.3. Governing Equation for Free Vibration Analysis

The time derivative of velocity at any given point within the element may be expressed in terms of the mid-surface displacement parameters (u_0 , v_0 and w_0) as

$$\frac{\partial^2}{\partial t^2} \left\{ \bar{f} \right\} = -\omega^2 \begin{Bmatrix} u_0 \\ v_0 \\ w_0 \end{Bmatrix} = -\omega^2 [F] \{f\}, \quad (27)$$

where the vector $\{f\}$ represents the nodal unknowns, which is of the 7×1 order and contains the terms of Equation (7).

The nodal unknowns $\{f\}$ are decoupled into a matrix $[C]$ that involves the shape functions (N_i) and global displacement vector $\{X\}$:

$$\{f\} = [C] \{X\}, \quad (28)$$

where the matrix $\{X\}$ contains the nodal unknowns of the nine nodes.

By utilizing the Equations (27) and (28), the mass matrix of an element can be written as

$$[m] = \iint_A [C]^T [L] [C] dA, \quad (29)$$

where the expression of the matrix $[L]$ can be expressed as

$$[L] = \int_z \rho [F]^T [F] dz, \quad (30)$$

where ρ is termed as the density of the CNT-reinforced rhombic plate. The derivation of element stiffness matrix and the mass matrix is given in the Appendix A. Hence, the governing equation for free vibration analysis of rhombic plate becomes

$$([K] - \omega^2 [M]) \{X\} = \{0\}, \quad (31)$$

where $[K]$ and $[M]$ are the linear stiffness matrix and mass matrix, respectively.

4.4. Skew Boundary Transformation

For the rhombic plate shown in Figure 2, it is important to alter the element matrices from global axes (x , y) to local axes (x' , y') because the skew boundary of the laminate is not parallel to the global

axes of the rhombic laminate. Hence, the transformation matrix $[T]$ is required at the element level to transform the element matrices from global to local axes.

$$\text{Transformation matrix } [T] = \begin{pmatrix} c & -s & 0 & 0 & 0 & 0 & 0 \\ s & c & 0 & 0 & 0 & 0 & 0 \\ 0 & 0 & 1 & 0 & 0 & 0 & 0 \\ 0 & 0 & 0 & c & -s & 0 & 0 \\ 0 & 0 & 0 & s & c & 0 & 0 \\ 0 & 0 & 0 & 0 & 0 & c & -s \\ 0 & 0 & 0 & 0 & 0 & s & c \end{pmatrix}, \quad (32)$$

where $c = \cos\alpha$, $s = \sin\alpha$ and α is the skew angle of the plate.

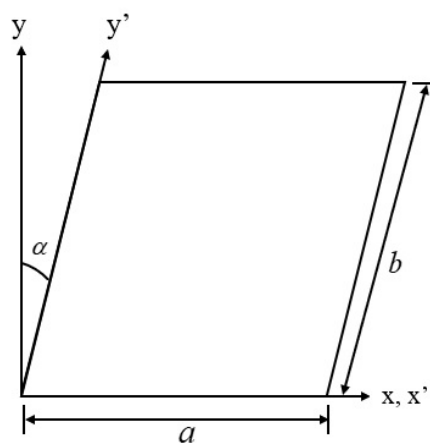


Figure 2. The coordinate system of the rhombic plate.

5. Numerical Results and Discussion

The static and free vibration analyses were performed for FG-CNT-reinforced rhombic plate under different combination of end support, volume fraction, and several geometric parameters. The above-discussed formulation has been incorporated into a computer code. The nine-noded isoparametric elements with seven degrees of freedom per node were chosen for the present model for discretizing the FG-CNT-reinforced rhombic plate. Poly{(m-phenylenevinylene)-co-[2,5-diethoxy-p-phenylene] vinylene}], basically known as PmPV [40], was chosen as the matrix and the armchair (10, 10) SWCNTs were considered as the reinforcing material. The material properties of the matrix were taken as $E^m = 2.1 \text{ GPa}$, $\rho^m = 1150 \text{ kg/m}^3$ and $\nu^m = 0.34$ at room temperature (300 K). The material properties of (10,10) SWCNTs at 300K are tabulated in Table 1. Three types volume fraction were used in present study. In the case of $V^*_{\text{CNT}} = 0.11$, $\eta_1 = 0.934$ and $\eta_2 = 0.149$, in the case of $V^*_{\text{CNT}} = 0.14$, $\eta_1 = 0.150$ and $\eta_2 = 0.941$, and for $V^*_{\text{CNT}} = 0.17$, $\eta_1 = 0.149$ and $\eta_2 = 1.381$. We assume that $\eta_2 = \eta_3$ and $G_{12} = G_{13} = G_{23}$. The abovementioned values are used for the following numerical results.

Table 1. Temperature-dependent material properties of (10, 10) SWCNT ($L = 9.26 \text{ nm}$, $R = 0.68 \text{ nm}$, $h = 0.067 \text{ nm}$, $\rho_{12}^{\text{CNT}} = 0.175$).

Temperature (K)	E_{11}^{CNT} (TPa)	E_{22}^{CNT} (TPa)	G_{12}^{CNT} (TPa)	ff_{11}^{CNT} ($10^{-6}/\text{K}$)	ff_{22}^{CNT} ($10^{-6}/\text{K}$)
300	5.6466	7.0800	1.9445	3.4584	5.1682
500	5.5308	6.9348	1.9643	4.5361	5.0189
700	5.4744	6.8641	1.9644	4.6677	4.8943

The non-dimensional quantities used are:

- For the bending analysis

$$\bar{w} = \frac{w}{h}, \bar{\sigma}_x = \sigma_x \left(\frac{a}{2}, \frac{b}{2}, z \right) \frac{h^2}{q_0 a^2}. \quad (33)$$

- For the free vibration analysis

$$\bar{\omega} = \omega \left(a^2/h \right) \sqrt{\rho^m/E^m}. \quad (34)$$

The loading patterns used for the bending analysis are:

For uniform loading $q = q_0$;

For sin-sin loading $q = q_0 \sin\left(\frac{\pi x}{a}\right) \sin\left(\frac{\pi y}{b}\right)$; (35)

For cos-cos loading $q = q_0 \cos\left(\frac{\pi x}{a}\right) \cos\left(\frac{\pi y}{b}\right)$.

The boundary conditions taken in the present analysis are as mentioned below:

1. Simply supported (SSSS):

$$v = w = \theta_y = \psi_y = 0 \text{ at } x = 0, a$$

$$u = w = \theta_x = \psi_x = 0 \text{ at } y = 0, b.$$

2. Clamped (CCCC):

$$u = v = w = \theta_x = \theta_y = \psi_x = \psi_y = 0 \text{ at } x = 0, a \text{ and } y = 0, b.$$

3. Clamped and simply supported (CCSS):

$$u = v = w = \theta_x = \theta_y = \psi_x = \psi_y = 0 \text{ at } x = 0, a$$

$$u = w = \theta_x = \psi_x = 0 \text{ at } y = 0, b.$$

5.1. Convergence and Validation of Present Formulation

5.1.1. Free Vibration Analysis

Example 1. The convergence study for the non-dimensional frequency parameter was carried out for UD and FG-CNT-reinforced rhombic plate shown in Table 2. The dimensionless frequency parameter of the UD, FG-V, FG-O, and FG-X type distributed CNTRC rhombic plate was computed for different mesh sizes and clamped boundary conditions. The results were computed for $V^*_{\text{CNT}} = 0.11$ and a skew angle of 15° . The convergence study indicated that 16×16 mesh is satisfactory for the free vibration analysis of functionally graded CNTRC rhombic plate using current nine-noded isoparametric elements. Hence, 16×16 mesh size was adopted for all the cases of free vibration analysis of a functionally graded CNT-reinforced rhombic plate.

Table 2. Convergence of non-dimensional frequency of FG-CNT-reinforced clamped rhombic plate.

Mesh	UD	FG-V	FG-O	FG-X
8×8	18.5932	18.0731	16.6424	19.2637
10×10	18.5915	18.0719	16.4112	19.2623
12×12	18.5906	18.0709	16.4093	19.2612
14×14	18.5894	18.0697	16.4085	19.2606
16×16	18.5892	18.0694	16.4084	19.2604

Example 2. Tables 3 and 4 show the results of the bending and free vibration analyses for an isotropic square plate ($\nu = 0.3$), respectively. The maximum deflection and axial stress were compared with the results provided by Reddy [41] and the frequency parameter of the isotropic plate was compared with an exact solution [42] and HSDT results for a moderately thick plate [43].

Table 3. Comparison of non-dimensional maximum deflection and normal stress of square isotropic plate subjected to uniform load.

a/h	Source	\bar{w}	$\bar{\sigma}_x$
10	Present	4.666	0.289
	Reddy [41]	4.770	0.289
20	Present	4.491	0.287
	Reddy [41]	4.570	0.268
50	Present	4.408	0.284
	Reddy [41]	4.496	0.266

Table 4. Comparison of non-dimensional frequency parameter of the simply supported square isotropic plate.

	Source	Mode		
		(1, 1)	(1, 2)	(1, 3)
	Present	0.093	0.221	0.415
	Mantari et al. [43]	0.093	0.222	0.415
	Srinivas et al. [42]	0.093	0.223	0.417

Example 3. Free vibration analyses of the FG-V CNT-reinforced composite plate for various a/h ratios were presented in Tables 5 and 6. The first six non-dimensional frequencies were compared with Zhu et al. [5]. Three volume fractions ($V^*_{\text{CNT}} = 0.11$ and 0.14) and three side-to-thickness ratios ($a/h = 10$, 20 and 50) were taken for comparison. The frequency parameter of simply supported and clamped boundary condition was found to be closer to Zhu et al. [5].

Table 5. Comparison study of first six non-dimensional frequency parameter of UD CNT-reinforced composite plate.

BC	V^*_{CNT}	Mode	$a/h = 10$		$a/h = 20$		$a/h = 50$	
			Zhu et al. [5]	Present	Zhu et al. [5]	Present	Zhu et al. [5]	Present
CCCC	0.11	1	17.625	18.284	28.400	29.232	39.730	41.246
		2	23.041	23.793	33.114	34.108	43.876	45.501
		3	33.592	34.188	44.559	45.456	54.768	56.313
		4	33.729	35.188	59.198	60.708	74.488	75.080
		5	37.011	38.536	61.851	63.003	98.291	100.577
		6	37.317	38.738	63.043	63.553	100.537	101.437
	0.14	1	18.127	18.854	29.911	30.795	43.583	45.216
		2	23.572	24.374	34.516	35.558	47.479	49.218
		3	34.252	34.874	45.898	46.830	57.968	59.617
		4	34.650	36.267	61.628	63.337	77.395	78.064
		5	37.921	39.384	64.199	64.457	106.371	104.359
		6	37.972	39.592	64.496	66.100	106.487	108.807
SSSS	0.11	1	13.532	13.885	17.355	18.014	19.223	20.124
		2	17.700	18.199	21.511	22.278	23.408	24.396
		3	19.449	19.422	32.399	33.231	34.669	35.734
		4	19.449	19.427	38.898	38.844	54.043	54.658
		5	27.569	28.121	38.898	38.854	70.811	73.189
		6	32.563	33.291	50.199	50.524	72.900	75.313
	0.14	1	14.306	14.668	18.921	19.618	21.354	22.359
		2	18.362	18.870	22.867	23.666	25.295	26.373
		3	19.791	19.769	33.570	34.419	36.267	37.393
		4	19.791	19.774	39.583	39.538	55.608	56.238
		5	28.230	28.784	39.583	39.548	78.110	80.675
		6	33.646	34.492	51.422	51.737	80.015	82.137

Table 6. Comparison study of first six non-dimensional frequency parameter of FG-V CNT-reinforced composite plate.

BC	V^*_{CNT}	Mode	$a/h = 10$		$a/h = 20$		$a/h = 50$	
			Zhu et al. [5]	Present	Zhu et al. [5]	Present	Zhu et al. [5]	Present
CCCC	0.11	1	17.211	17.753	26.304	26.693	34.165	34.480
		2	22.812	23.462	31.496	32.099	39.043	39.584
		3	33.070	34.035	43.589	44.133	51.204	51.815
		4	33.552	34.355	56.249	57.061	72.202	71.954
		5	36.528	37.889	59.249	60.253	86.291	86.133
		6	37.437	38.841	62.608	62.218	89.054	89.105
	0.14	1	17.791	18.405	27.926	28.371	37.568	37.909
		2	23.413	24.113	32.976	33.629	42.175	42.733
		3	34.101	34.792	44.989	45.573	53.963	54.590
		4	34.275	35.553	58.951	59.968	74.785	74.546
		5	37.538	39.053	61.816	63.051	94.022	93.911
		6	38.159	39.574	64.135	63.758	96.573	96.680
SSSS	0.11	1	12.452	12.601	15.110	15.291	16.252	16.465
		2	17.060	17.409	19.903	20.297	21.142	21.573
		3	19.499	19.479	31.561	32.106	33.350	33.993
		4	19.499	19.484	38.998	38.959	53.430	53.670
		5	27.340	27.762	38.998	38.969	60.188	60.337
		6	31.417	31.903	47.739	47.899	62.198	63.042
	0.14	1	13.256	13.415	16.510	16.701	17.995	18.228
		2	17.734	18.090	21.087	21.483	22.643	23.082
		3	19.879	19.871	32.617	33.163	34.660	35.306
		4	19.879	19.876	39.759	39.742	54.833	55.062
		5	28.021	28.449	39.759	39.752	66.552	66.712
		6	32.678	33.284	51.078	51.122	68.940	69.212

5.1.2. Bending Analysis

Example 4. Table 7 depicts the convergence study for dimensionless maximum deflection for UD and FG-CNT-reinforced functionally graded rhombic plate. The dimensionless maximum deflection of the UD, FG-V, FG-O and FG-X CNTRC rhombic plate was computed for different mesh size and clamped boundary condition. The results were computed for $V^*_{\text{CNT}} = 0.11$. The convergence study showed that 16×16 mesh size is acceptable for the present model using the discussed nine-noded isoparametric elements. Hence, 16×16 mesh size was chosen for all the parametric studies of the bending analysis of functionally graded CNTRC rhombic plate.

Table 7. Convergence of non-dimensional maximum deflection of CNT-reinforced functionally graded clamped rhombic plate.

Mesh	UD	FG-V	FG-O	FG-X
8 × 8	0.00372	0.00422	0.00588	0.00309
10 × 10	0.00361	0.00411	0.00576	0.00297
12 × 12	0.00355	0.00406	0.00568	0.00292
14 × 14	0.00349	0.00402	0.00561	0.00289
16 × 16	0.00345	0.00401	0.00557	0.00287

Example 5. The dimensionless central deflection (w/h) of the uniformly distributed CNT-reinforced composite plate with different side-to-thickness ratios and end supports were presented in Tables 8 and 9. The non-dimensional central deflection was compared with Zhu et al. [5]; $V^*_{\text{CNT}} = 0.11, 0.14$ and $a/h = 10, 20, 50$ were used for the comparison study. The dimensionless central deflection of different types of boundary condition was found to be in decent agreement with Zhu et al. [5].

Table 8. Comparison study of non-dimensional maximum deflection of various volume fraction of UD CNT-reinforced composite plate.

BC	V^*_{CNT}	$a/h = 10$		$a/h = 20$		$a/h = 50$	
		Zhu et al. [5]	Present	Zhu et al. [5]	Present	Zhu et al. [5]	Present
CCCC	0.11	0.00222	0.00207	0.01339	0.01257	0.2618	0.24056
	0.14	0.00208	0.00192	0.01188	0.01115	0.2131	0.19644
SSSS	0.11	0.00373	0.00354	0.03628	0.03352	1.1550	1.04729
	0.14	0.00330	0.00314	0.03001	0.02779	0.9175	0.83205
SCSC	0.11	0.00332	0.00313	0.03393	0.03127	1.0990	0.99624
	0.14	0.00297	0.00281	0.02852	0.02634	0.8890	0.80555
SFSF	0.11	0.00344	0.00339	0.03341	0.03223	1.0680	1.01428
	0.14	0.00302	0.00297	0.02760	0.02654	0.8505	0.80295

Table 9. Comparison study of non-dimensional maximum deflection of various volume fraction of UD CNT-reinforced composite plate.

BC	V^*_{CNT}	$a/h = 10$		$a/h = 20$		$a/h = 50$	
		Zhu et al. [5]	Present	Zhu et al. [5]	Present	Zhu et al. [5]	Present
CCCC	0.11	0.00211	0.00191	0.01150	0.01052	0.18940	0.16721
	0.14	0.00198	0.00179	0.01036	0.00954	0.15600	0.13941
SSSS	0.11	0.00318	0.00294	0.02701	0.02398	0.79000	0.67655
	0.14	0.00284	0.00266	0.02256	0.02021	0.62710	0.53777
SCSC	0.11	0.00286	0.00264	0.02587	0.02297	0.77280	0.66351
	0.14	0.00258	0.00240	0.02184	0.01955	0.62060	0.53313
SFSF	0.11	0.00290	0.00276	0.02484	0.02281	0.73380	0.70308
	0.14	0.00259	0.00248	0.02078	0.01916	0.58540	0.54605

5.2. Results and Discussion

The comparison study indicates that the present mathematical model and its finite element implementation results are in agreement with the previously published results. The present study has been conducted to investigate the effect of loading pattern, side-to-thickness ratios (a/h), aspect ratio (a/b), skew angle (α), volume fraction of CNT (V^*_{CNT}), and different boundary conditions (SSSS, CCCC, CCSS, CSCS, CCFF, and CFCF) on the bending and free vibration behavior of functionally graded CNT-reinforced composite rhombic plate.

5.2.1. Free Vibration Analysis

Tables 10 and 11 represent the first six dimensionless frequency parameter of UD-CNT- and FG-CNT-reinforced rhombic plate for the three different types of CNT volume fraction ($V^*_{\text{CNT}} = 0.11, 0.14$ and 0.17) and four different skew angles ($\alpha = 15^\circ, 30^\circ, 45^\circ$ and 60°). The results were tabulated for simply supported and clamped boundary condition, respectively. It was noticed that an increase in the skew angle results in an increase in dimensionless frequency parameter for all types of CNTs distribution and all considered CNT volume fractions. An approximately 6% increase was noticed in the dimensionless fundamental frequency parameter of functionally graded CNTRC rhombic plate when skew angle changes from 15° to 30° , 22% and 60% increase was noticed for 15° to 45° and for 15° to 60° . Table 12 shows the dimensionless frequency parameter of FG-CNTRC-reinforced rhombic plate for CCSS-, CSCS-, CCFF-, and CFCF-type boundary support. For the all considered boundary conditions and skew angles, the FG-O distribution retains the minimum dimensionless frequency parameter while the FG-X distribution shows maximum values of dimensionless frequency parameter among other kinds of distribution. Additional distribution of CNTs should be provided at the top and the bottom section rather than at the mid-section for attaining maximum stiffness.

Table 10. Variation of first six natural non-dimensional frequency parameters of simply supported FG-CNT-reinforced rhombic plate.

Types	V^*_{CNT}	Skew Angle	Mode					
			1	2	3	4	5	6
UD	0.11	15°	14.0884	18.3200	18.8946	22.6183	29.3328	33.6414
		30°	14.8977	18.8299	21.3717	28.4322	33.1078	35.1178
		45°	17.1862	20.5115	26.9900	37.0144	39.6322	39.6568
		60°	22.7998	24.0366	38.2235	46.2487	47.8936	50.9246
	0.14	15°	14.8687	18.6487	19.5642	23.0233	30.0198	34.8422
		30°	15.6755	19.1758	22.0498	28.9455	33.9035	36.3247
		45°	17.9727	20.9102	27.7332	37.7063	40.6588	40.8949
		60°	23.2808	24.8769	39.2472	47.5170	49.0156	52.2774
	0.17	15°	17.4811	22.9180	23.5104	28.2964	36.5676	41.9224
		30°	18.4931	23.5450	26.6092	35.5615	41.2831	43.7657
		45°	21.3530	25.6345	33.6340	46.2801	49.4285	49.4321
		60°	28.4860	29.9161	47.6618	57.6946	59.7955	63.5234
FG-V	0.11	15°	12.8212	18.1269	18.3759	22.6786	28.9595	32.2712
		30°	13.6868	18.8528	20.6993	28.4857	32.6175	33.8100
		45°	16.0825	20.5023	26.3727	36.9725	38.5706	38.8945
		60°	22.7651	23.1363	37.4158	45.9406	47.6860	50.0097
	0.14	15°	13.6306	18.7223	18.8344	23.1366	29.6827	33.6486
		30°	14.4859	19.2484	21.3970	29.0713	33.4956	35.1799
		45°	16.8766	20.9596	27.1726	37.8010	39.9021	40.0565
		60°	23.3107	23.9748	38.5628	47.3845	48.9510	51.4979
	0.17	15°	15.8726	22.5869	23.1041	28.5207	36.1984	40.2043
		30°	16.9639	23.7009	25.8142	35.8176	40.7628	42.1365
		45°	19.9783	25.7658	32.9286	46.4775	48.1150	48.5974
		60°	28.6027	28.8423	46.7338	57.6186	59.8787	62.5277
FG-O	0.11	15°	11.2246	16.8568	18.2727	22.5605	27.7024	28.6900
		30°	12.1133	18.7752	19.3640	28.3558	30.3139	30.7798
		45°	14.5197	20.4388	24.7329	35.2696	36.2118	36.9006
		60°	21.5223	22.7001	34.8852	45.8698	46.6015	47.6229
	0.14	15°	11.9547	17.3832	18.6042	22.9689	28.2193	30.0605
		30°	12.8181	19.1248	19.9022	28.8740	31.5416	31.6441
		45°	15.1892	20.8433	25.3918	36.4990	37.2763	37.6006
		60°	22.1785	23.1888	35.8993	47.2005	47.9486	48.7680
	0.17	15°	13.8793	20.7785	22.8791	22.8791	34.1824	35.9124
		30°	14.9671	23.4971	23.8865	35.4973	37.8814	38.1425
		45°	17.9248	25.5652	30.5918	43.9152	45.0463	46.1779
		60°	26.5756	28.3845	43.3295	57.2497	58.0859	59.5035
FG-X	0.11	15°	15.3579	18.4618	19.9956	22.7929	30.4082	35.0962
		30°	16.1745	18.9803	22.4702	28.6545	34.2453	36.6028
		45°	18.4949	20.6851	28.1124	37.3147	40.9182	41.2241
		60°	23.0073	25.4117	39.5510	46.7919	48.3756	52.4841
	0.14	15°	16.0673	18.8614	20.7220	23.2855	31.2995	36.1529
		30°	16.9039	19.3980	23.2367	29.2774	35.2156	37.6988
		45°	19.2847	21.1602	28.9762	38.1470	42.0428	42.4396
		60°	23.5712	26.3605	40.6662	48.1906	49.6636	53.9309
	0.17	15°	19.0583	23.2864	25.1259	28.7507	38.4760	43.6385
		30°	20.1180	23.9280	28.2892	36.1352	43.2193	45.5938
		45°	23.1055	26.0614	35.4283	47.0376	51.4225	51.5545
		60°	28.9750	31.9346	49.7188	58.8146	60.8682	65.8386

Table 11. Variation of first six natural non-dimensional frequency parameters of clamped FG-CNT-reinforced rhombic plate.

Types	V^*_{CNT}	Skew Angle	Mode					
			1	2	3	4	5	6
UD	0.11	15°	18.5892	24.6235	35.3293	35.6482	39.8059	40.1566
		30°	19.7907	27.5192	37.5758	38.7334	44.7699	44.8668
		45°	23.1240	33.7718	43.5280	45.2188	54.8007	56.3342
		60°	32.8768	46.6645	58.8579	62.5042	70.8589	76.4394
	0.14	15°	19.1594	25.2162	36.0641	36.7261	40.8256	40.8465
		30°	20.3677	28.1613	38.6503	39.6187	45.6147	45.7882
		45°	23.7315	34.5566	44.6059	46.2941	55.7146	57.5412
		60°	33.6101	47.7344	60.1998	63.7591	72.4446	77.7145
	0.17	15°	23.1763	30.7160	44.0894	44.4545	49.6574	50.1117
		30°	24.6779	34.3325	46.8674	48.3332	55.8713	55.9847
		45°	28.8430	42.1399	54.3158	56.4308	68.3713	70.3186
		60°	41.0318	58.2465	73.4787	78.0518	88.4742	95.3523
FG-V	0.11	15°	18.0694	24.2993	34.8395	35.1140	39.2444	40.2623
		30°	19.3073	27.1997	36.8576	38.3514	44.4246	44.9823
		45°	22.7117	33.3930	43.0375	44.7306	54.9298	55.8898
		60°	32.5888	46.2233	58.3954	62.3472	70.4436	76.6148
	0.14	15°	18.7213	24.9627	35.9325	36.0340	40.3826	41.0223
		30°	19.9628	27.9173	38.0427	39.3412	45.5331	45.8315
		45°	23.3936	34.2698	44.2154	45.9247	55.9691	57.3257
		60°	33.3992	47.4078	59.8831	63.7136	72.2043	78.0564
	0.17	15°	22.5493	30.3816	43.5223	43.9471	49.0751	50.5020
		30°	24.1057	34.0165	46.0643	47.9801	55.5987	56.4159
		45°	28.3819	41.7701	53.8425	55.9614	68.8770	69.9530
		60°	40.7818	57.8482	73.1009	78.1001	88.2112	96.0396
FG-O	0.11	15°	16.4084	22.9046	31.6159	33.6029	36.6562	40.0537
		30°	17.7077	25.7508	33.8501	36.2830	42.3527	44.7506
		45°	21.2099	31.6586	40.5674	42.2311	52.8152	53.9899
		60°	31.2046	44.1065	55.5461	60.6186	66.8835	76.2352
	0.14	15°	17.0452	23.4601	32.8241	34.3062	37.6525	40.7285
		30°	18.3275	26.3574	34.9993	37.1966	43.2631	45.5052
		45°	21.8175	32.4388	41.6106	43.3410	54.1879	55.1259
		60°	31.8862	45.1773	56.9465	61.7865	68.6013	77.5228
	0.17	15°	20.4935	28.4369	39.6386	41.7340	45.7071	50.0278
		30°	22.0844	31.9798	42.3651	45.1869	52.6957	55.8895
		45°	26.3966	39.3908	50.6104	52.6850	65.9841	67.2724
		60°	38.8088	55.0062	69.4149	75.5700	83.7054	95.1822
FG-X	0.11	15°	19.2604	25.3608	36.1914	36.8063	40.4675	40.9340
		30°	20.4754	28.2998	38.7220	39.7120	45.2151	45.8357
		45°	23.8434	34.6543	44.6261	46.3103	55.2276	57.4279
		60°	33.6486	47.6758	59.9923	63.4780	72.0668	77.0374
	0.14	15°	19.8084	26.0430	37.1106	37.8532	41.2910	42.0442
		30°	21.0506	29.0493	39.8008	40.7351	46.1353	47.0096
		45°	24.4920	35.5521	45.7961	47.4919	56.3516	58.8017
		60°	34.4934	48.8548	61.4386	64.9465	73.7658	78.6049
	0.17	15°	24.0671	31.9338	45.6821	45.9560	50.9173	51.3375
		30°	25.6288	35.6476	48.4261	49.9805	56.8856	57.6593
		45°	29.9300	43.6056	55.9981	58.1580	69.4729	72.2037
		60°	42.3389	59.8760	75.2616	79.8475	90.3762	96.8913

Table 12. Variation of fundamental natural non-dimensional frequency parameters of FG-CNT-reinforced rhombic plate.

Types	V^*_{CNT}	Skew Angle	Boundary Condition			
			CCSS	CSCS	CCFF	CFCF
UD	0.11	15°	17.5656	16.1325	17.1211	5.8025
		30°	18.3524	17.1106	17.4540	5.8490
		45°	20.7007	19.8447	18.4603	5.9919
		60°	28.2486	27.7948	21.7009	6.3069
		15°	18.1342	16.7688	17.7012	6.2424
		30°	18.9229	17.7494	18.0355	6.2905
	0.14	45°	21.2864	20.5072	19.0480	6.4353
		60°	28.9146	28.5757	22.3161	6.7554
		15°	21.8982	20.0801	21.3412	7.1743
		30°	22.8820	21.3025	21.7584	7.2326
		45°	25.8166	24.7178	23.0172	7.4116
		60°	35.2478	34.6467	27.0680	7.8059
FG-V	0.11	15°	17.0086	15.3184	16.5114	5.0487
		30°	17.8273	16.3356	16.8584	5.0936
		45°	20.2441	19.1336	17.8998	5.2408
		60°	27.9303	27.1387	21.2303	5.5617
		15°	17.6618	16.0166	17.1825	5.4678
		30°	18.4787	17.0329	17.5285	5.5141
	0.14	45°	20.9045	19.8505	18.5709	5.6624
		60°	28.6673	27.9750	21.9207	5.9884
		15°	21.2161	19.0620	20.5857	6.2207
		30°	22.2464	20.3420	21.0234	6.2774
		45°	25.2838	23.8570	22.3339	6.4629
		60°	34.9349	33.9038	26.5208	6.8657
FG-O	0.11	15°	15.2966	13.7187	14.7110	4.3016
		30°	16.1749	14.7745	15.0980	4.3467
		45°	18.6942	17.6072	16.2095	4.4929
		60°	26.5093	25.5699	19.6311	4.7975
		15°	15.9573	14.3811	15.4087	4.6680
		30°	16.8163	15.4187	15.7844	4.7147
	0.14	45°	19.3078	18.2378	16.8762	4.8622
		60°	27.1313	26.2562	20.2771	5.1739
		15°	19.1484	17.0768	18.4438	5.2956
		30°	20.2204	18.3681	18.9177	5.3519
		45°	23.3092	21.8497	20.2813	5.5337
		60°	32.9609	31.7016	24.4972	5.9132
FG-X	0.11	15°	18.2140	17.0254	17.7792	6.5860
		30°	19.0078	18.0146	18.1123	6.6352
		45°	21.3832	20.7913	19.1261	6.7811
		60°	29.0061	28.8746	22.3997	7.1022
		15°	18.7355	17.6246	18.2942	7.0150
		30°	19.5470	18.6364	18.6340	7.0670
	0.14	45°	21.9758	21.4797	19.6696	7.2180
		60°	29.7641	29.7602	23.0163	7.5489
		15°	22.7038	21.2134	22.1242	8.1485
		30°	23.7285	22.4908	22.5506	8.2111
		45°	26.7784	26.0495	23.8494	8.3974
		60°	36.4902	36.3121	28.0370	8.8055

Therefore, the FG-X and FG-O distributions yield maximum and minimum stiffness, respectively. Apart from this, the CCCC end support yields the highest dimensionless frequency parameter while the CFCF end support shows the lowest value among all considered boundary condition resulting from the fact that the higher constraints at support impart higher stiffness to the FG-CNTRC rhombic plate. The effect of the side-to-thickness ratio for various types of skew angles was presented in Table 13. The dimensionless fundamental frequency parameter for all type of CNT distribution was

increased along with the a/h ratio. The dimensionless frequency parameter also increases with the aspect ratio of FG-CNTR-reinforced rhombic plate, as depicted in Figure 3. The results were calculated for skew angles of 15° and 30° . The first four mode shapes for FG-V CNT-reinforced rhombic square plate having simply supported boundary condition and 30° skew angle are presented in Figure 4.

Table 13. Variation of fundamental natural non-dimensional frequency parameters of FG-CNT-reinforced rhombic plate.

Types	V^*_{CNT}	Skew Angle	a/h			
			5	20	50	100
UD	0.11	15°	9.0743	18.2012	20.3073	20.6787
		30°	9.4150	18.9711	21.0669	21.4408
		45°	10.2558	21.3334	23.4743	23.8687
		60°	11.3999	29.4063	32.2438	32.8085
	0.14	15°	9.3243	19.7973	22.5305	23.0303
		30°	9.5879	20.5395	23.2468	23.7472
		45°	10.4551	22.8478	25.5594	26.0749
		60°	11.6404	30.8885	34.2574	34.9408
	0.17	15°	11.3132	22.4497	24.9546	25.3933
		30°	11.7725	23.4173	25.9121	26.3544
		45°	12.8172	26.3808	28.9389	29.4075
		60°	14.2430	36.4827	39.9125	40.5928
FG-V	0.11	15°	8.7986	15.5123	16.6902	16.8853
		30°	9.4269	16.4011	17.5995	17.8014
		45°	10.2475	19.0147	20.3313	20.5637
		60°	11.3736	27.4772	29.5441	29.9513
	0.14	15°	9.1228	16.9116	18.4397	18.6988
		30°	9.6238	17.7666	19.3058	19.5706
		45°	10.4761	20.3260	21.9636	22.2570
		60°	11.6465	28.7997	31.1984	31.6713
	0.17	15°	10.9766	19.0705	20.4470	20.6737
		30°	11.8498	20.1959	21.5996	21.8348
		45°	12.8769	23.4938	25.0480	25.3214
		60°	14.2886	34.1237	36.6062	37.0957
FG-O	0.11	15°	8.0040	13.1635	13.9508	14.0776
		30°	8.7975	14.0945	14.9077	15.0418
		45°	10.2194	16.7496	17.6897	17.8561
		60°	11.3501	25.0679	26.6826	27.0149
	0.14	15°	8.3081	14.3293	15.3437	15.5098
		30°	9.1008	15.2139	16.2464	16.4188
		45°	10.4216	17.7910	18.9359	19.1387
		60°	11.5944	26.0648	27.8938	28.2650
	0.17	15°	9.9887	16.1395	17.0377	17.1815
		30°	10.9641	17.2789	18.2081	18.3607
		45°	12.7826	20.5334	21.6118	21.8026
		60°	14.1922	30.7514	32.6180	33.0048
FG-X	0.11	15°	9.2309	21.2410	24.8589	25.5557
		30°	9.4901	21.9714	25.5444	26.2392
		45°	10.3425	24.2577	27.7886	28.4923
		60°	11.5036	32.2825	36.4515	37.3272
	0.14	15°	9.4307	22.9391	27.5913	28.5358
		30°	9.6990	23.6674	28.2521	29.1913
		45°	10.5801	25.9622	30.4437	31.3820
		60°	11.7856	34.0782	39.1212	40.2237
	0.17	15°	11.6432	26.2338	30.6098	31.4489
		30°	11.9640	27.1943	31.5188	32.3564
		45°	13.0307	30.1785	34.4733	35.3262
		60°	14.4875	40.5269	45.7146	46.8021

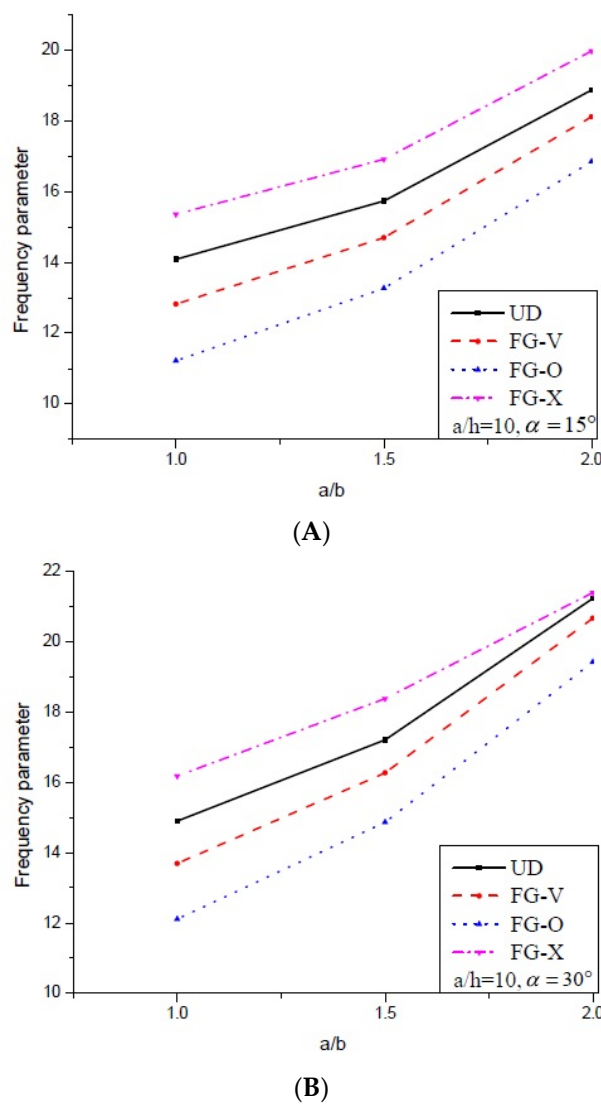


Figure 3. Variation of non-dimensional frequency parameter of FG-CNT-reinforced rhombic plate with aspect ratio; (A) $\alpha = 15^\circ$ and (B) $\alpha = 30^\circ$.

5.2.2. Static Analysis

The dimensionless maximum deflection of a FG-CNT-reinforced rhombic plate under uniform loading for simply supported and clamped boundary conditions is shown in Tables 14 and 15, respectively. The volume fraction of CNT was taken as 0.11, 0.14 and 0.17. The results were tabulated for UD and FG-CNT-reinforced rhombic plate with $a/b = 1$ and $a/h = 10$. It can be observed that an increase in the volume fraction of CNTs results in a decrease in the deflection of CNTRC rhombic plate because of the fact that the higher value of volume fraction has higher stiffness; thus, the deflection is reduced. It is anticipated that there is a nearly 36% decrease shown in maximum deflection for both clamped and simply supported boundary conditions as the value of V^*_{CNT} increases from 0.11 to 0.17 and approximately 6% decreases are noticed when V^*_{CNT} changes from 0.11 to 0.14. Maximum dimensionless deflection decreases with an increase in the skew angle because it reduces the length of the shorter diagonal leading to an enhancement in the stiffness of the rhombic plate. Thus, the deflection is reduced.

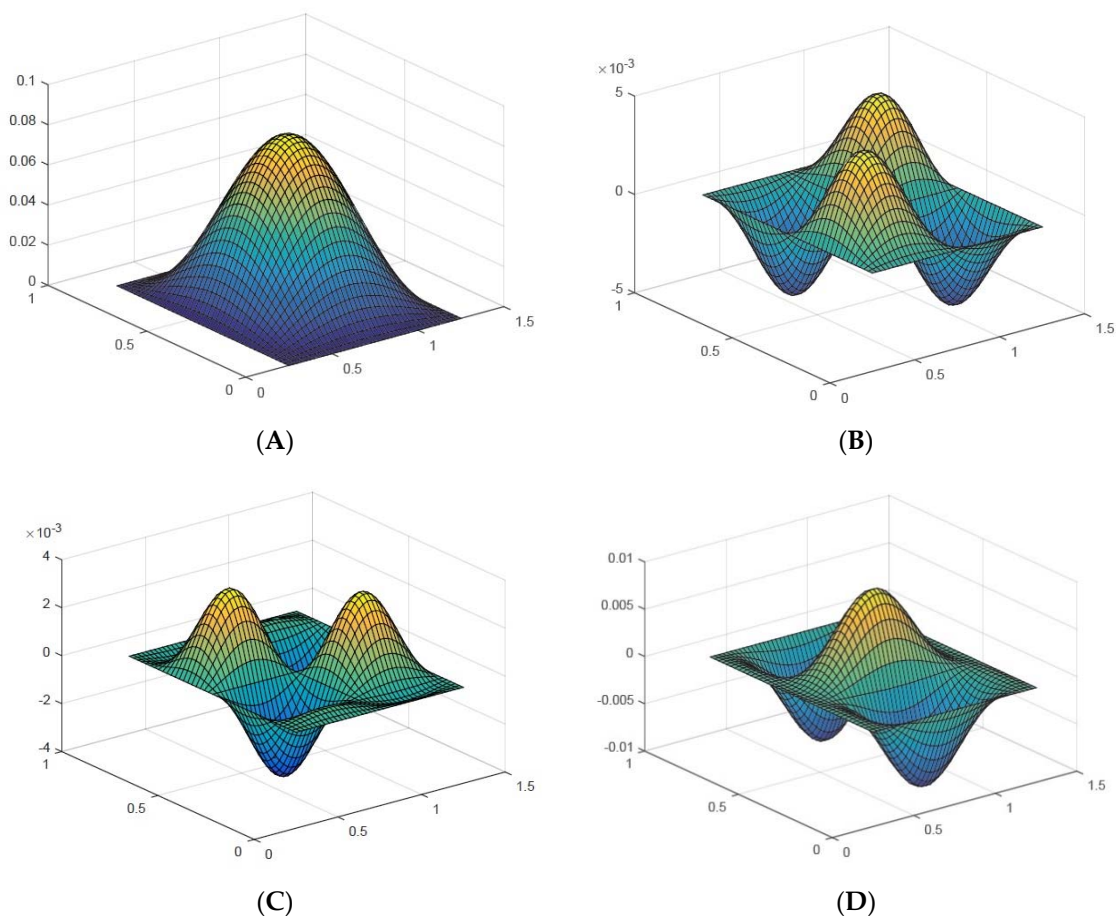


Figure 4. The free vibration mode shapes of a SSSS square FG-V CNT-reinforced rhombic plate for skew angle 30° (A) 1st Mode; (B) 2nd Mode; (C) 3rd Mode and (D) 4th Mode.

Table 14. Variation of non-dimensional maximum deflection of FG-CNT-reinforced simply supported rhombic plate under uniform loading.

Types	V^*_{CNT}	Skew Angle			
		15°	30°	45°	60°
UD	0.11	0.00345	0.00311	0.00234	0.00119
	0.14	0.00306	0.00278	0.00212	0.00110
	0.17	0.00222	0.00199	0.00150	0.00076
FG-V	0.11	0.00401	0.00365	0.00267	0.00128
	0.14	0.00354	0.00323	0.00240	0.00118
	0.17	0.00257	0.00234	0.00170	0.00081
FG-O	0.11	0.00557	0.00479	0.00333	0.00149
	0.14	0.00486	0.00424	0.00302	0.00140
	0.17	0.00360	0.00310	0.00216	0.00097
FG-X	0.11	0.00287	0.00261	0.00201	0.00106
	0.14	0.00260	0.00237	0.00183	0.00098
	0.17	0.00185	0.00167	0.00127	0.00066

Table 15. Variation of non-dimensional maximum deflection of FG-CNT-reinforced clamped rhombic plate under uniform loading.

Types	V^*_{CNT}	Skew Angle			
		15°	30°	45°	60°
UD	0.11	0.00201	0.00178	0.00131	0.00065
	0.14	0.00187	0.00167	0.00124	0.00061
	0.17	0.00127	0.00113	0.00083	0.00041
FG-V	0.11	0.00214	0.00189	0.00137	0.00066
	0.14	0.00197	0.00175	0.00128	0.00062
	0.17	0.00136	0.00120	0.00087	0.00042
FG-O	0.11	0.00263	0.00226	0.00158	0.00072
	0.14	0.00241	0.00210	0.00148	0.00069
	0.17	0.00166	0.00144	0.00101	0.00046
FG-X	0.11	0.00186	0.00166	0.00123	0.00061
	0.14	0.00174	0.00155	0.00116	0.00058
	0.17	0.00117	0.00104	0.00077	0.00038

Tables 16 and 17 represent the dimensionless maximum deflection of simply supported and clamped FG-CNT-reinforced rhombic plate under sin-sin loading, respectively. Here, an approximately 25% decrease in the maximum dimensionless deflection is noticed when the skew angle changes from 15° to 30°; 40% decreases when the skew angle changes from 30° to 45° and 55% decreases when the skew angle changes from 45° to 60° for both uniform loading and sin-sin loading. The lowest and highest dimensionless deflection was found for FG-O- and FG-X-type CNT distribution, respectively.

Table 16. Variation of non-dimensional maximum deflection of FG-CNT-reinforced simply supported rhombic plate under sin-sin loading.

Types	V^*_{CNT}	Skew Angle			
		15°	30°	45°	60°
UD	0.11	0.00215	0.00158	0.00092	0.00038
	0.14	0.00192	0.00142	0.00084	0.00036
	0.17	0.00138	0.00101	0.00059	0.00024
FG-V	0.11	0.00248	0.00183	0.00102	0.00040
	0.14	0.00220	0.00163	0.00093	0.00037
	0.17	0.00159	0.00117	0.00065	0.00026
FG-O	0.11	0.00339	0.00237	0.00126	0.00047
	0.14	0.00297	0.00211	0.00115	0.00044
	0.17	0.00219	0.00153	0.00081	0.00030
FG-X	0.11	0.00181	0.00135	0.00081	0.00035
	0.14	0.00165	0.00123	0.00074	0.00032
	0.17	0.00116	0.00086	0.00051	0.00022

Figure 5 shows the variation of dimensionless deflection of FG-V CNT-reinforced rhombic plate along the length (x/a) at $y/b = 0.50$ for four skew angles under sin-sin loading. It can be seen that all values of CNT volume fraction have the same nature of deflection along the length and for the skew angle 60°, negative deflection is noticed for the farther end subjected to sin-sin loading.

Table 17. Variation of non-dimensional maximum deflection of FG-CNT-reinforced clamped rhombic plate under sin-sin loading.

Types	V^*_{CNT}	Skew Angle			
		15°	30°	45°	60°
UD	0.11	0.00136	0.00101	0.00059	0.00025
	0.14	0.00127	0.00095	0.00056	0.00023
	0.17	0.00086	0.00064	0.00038	0.00016
FG-V	0.11	0.00145	0.00106	0.00062	0.00025
	0.14	0.00134	0.00099	0.00058	0.00024
	0.17	0.00092	0.00067	0.00039	0.00016
FG-O	0.11	0.00177	0.00128	0.00071	0.00027
	0.14	0.00163	0.00118	0.00067	0.00026
	0.17	0.00112	0.00081	0.00045	0.00017
FG-X	0.11	0.00126	0.00094	0.00056	0.00023
	0.14	0.00118	0.00088	0.00052	0.00022
	0.17	0.00080	0.00059	0.00035	0.00015

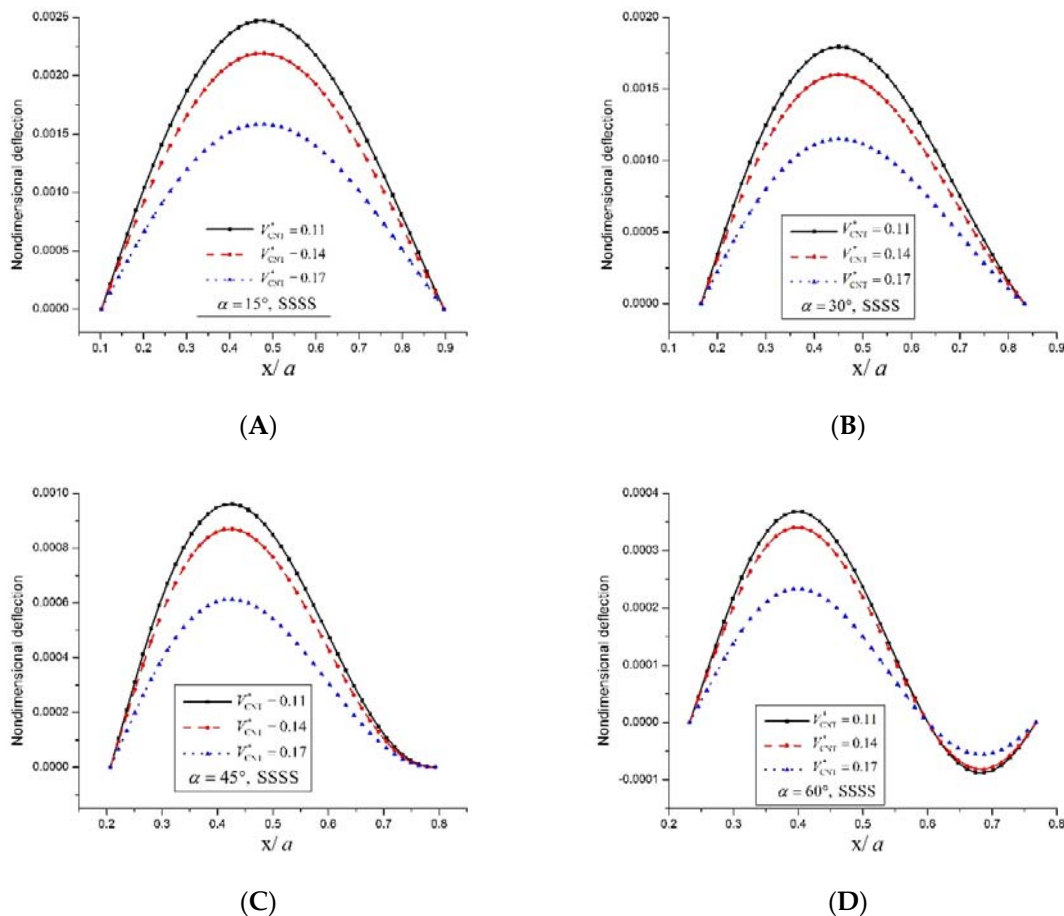


Figure 5. Non-dimensional deflection of FG-V CNT-reinforced rhombic plate along the central line for (A) 15° ; (B) 30° ; (C) 45° and (D) 60° skew angle subjected to sin-sin loading.

The effect of loading type on the non-dimensional deflection of simply supported and clamped FG-V type CNT-reinforced rhombic plate with skew angle was shown in Figure 6.

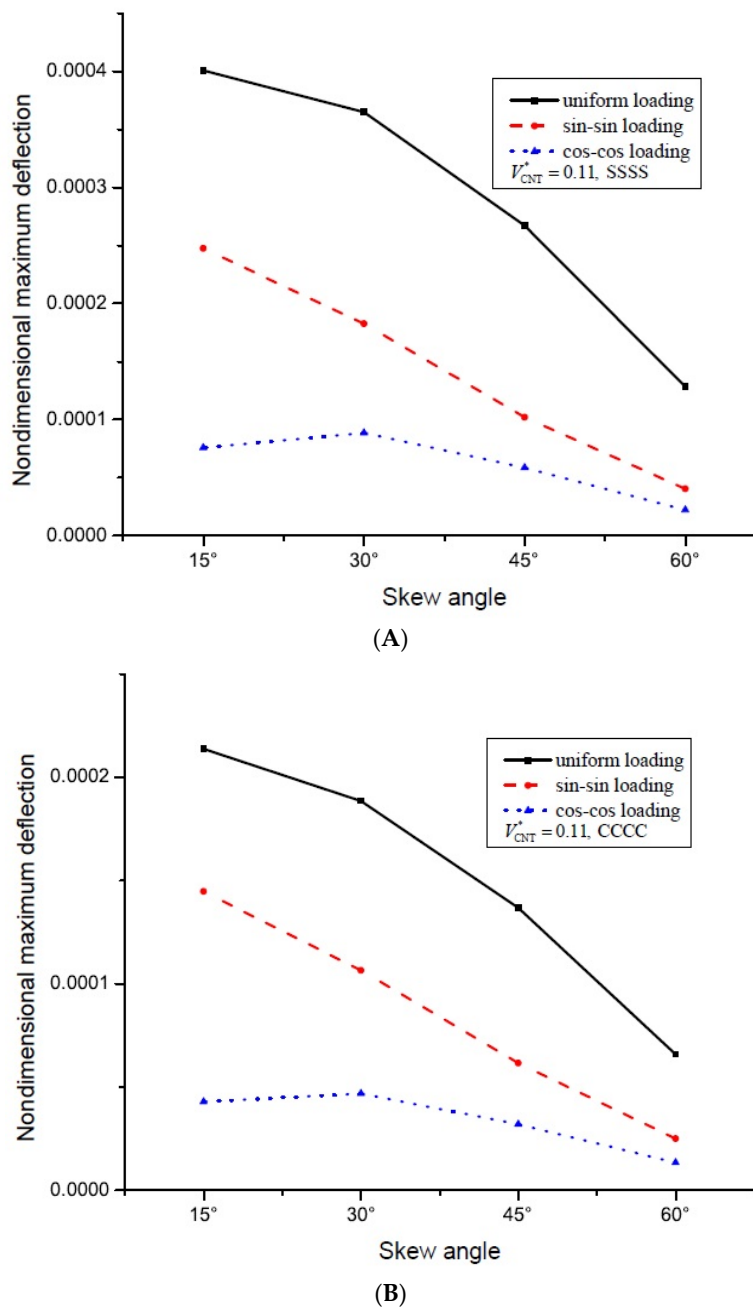


Figure 6. Variation of non-dimensional deflection of FG-V CNT-reinforced rhombic plate with the skew angle for (A) SSSS and (B) CCCC boundary condition.

The non-dimensional maximum deflection decreased with an increase in the skew angle for uniform and sin-sin loading, while under the cos-cos loading, the value of \bar{w} increases first and then decreases as the skew angle grows. The effect of the skew angle on the maximum dimensionless deflection of CNT-reinforced rhombic plate subjected to sin-sin loading having various types of boundary condition was shown in Figure 7. For all considered boundary conditions except CFCF, the pattern of dimensionless deflection along the skew angle is linear. Figure 8 shows the variation in dimensionless deflection of FG-CNT-reinforced rhombic plate along the length of the central line for four types of side-to-thickness ratios subjected to sin-sin load. The same nature of deflection along the length was noticed for all values of a/h . The results were calculated for the skew angle of 30° and simply supported boundary condition.

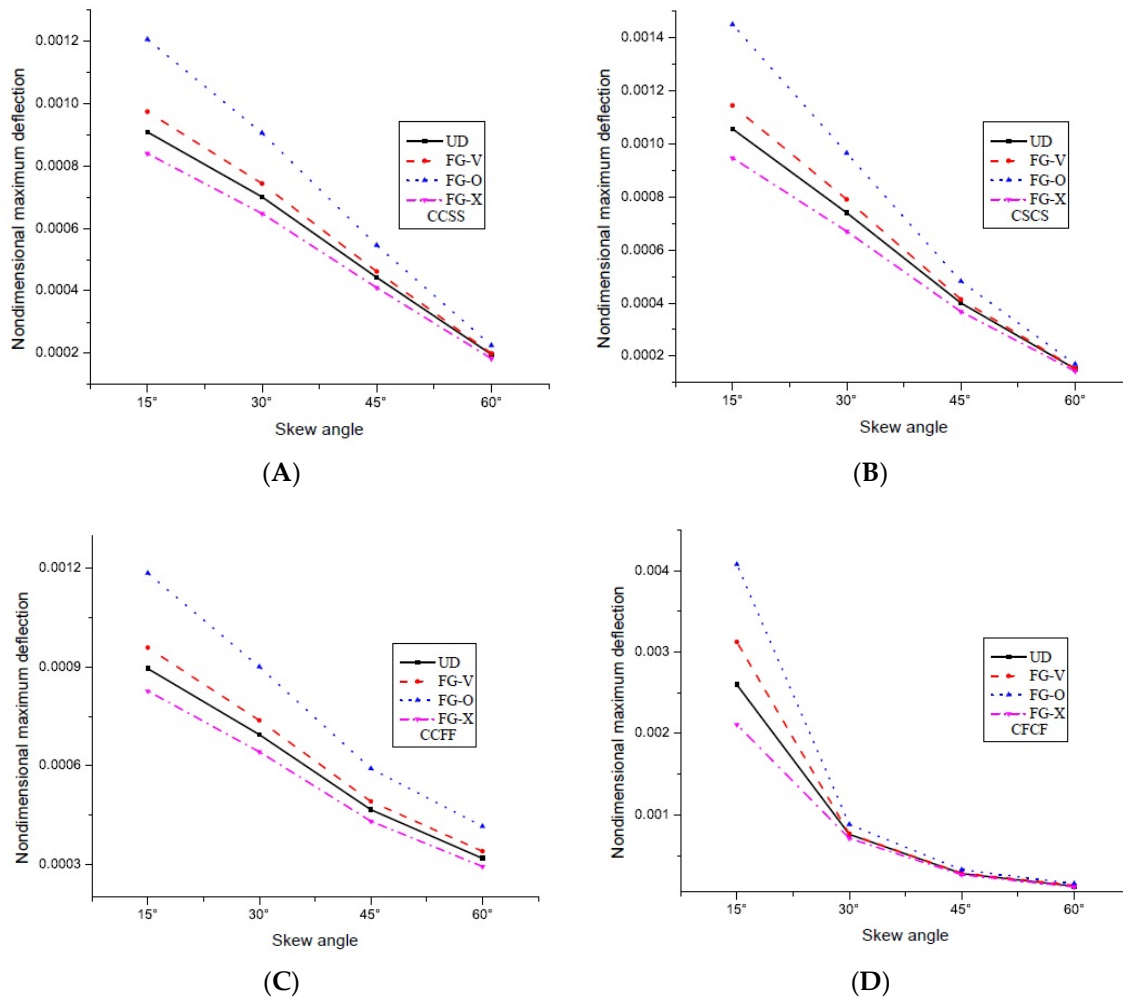


Figure 7. Variation of non-dimensional deflection of FG-CNT-reinforced rhombic plate with the skew angle subjected to sin-sin loading for (A) CCSS, (B) CSCS, (C) CCFF and (D) CFCF boundary condition.

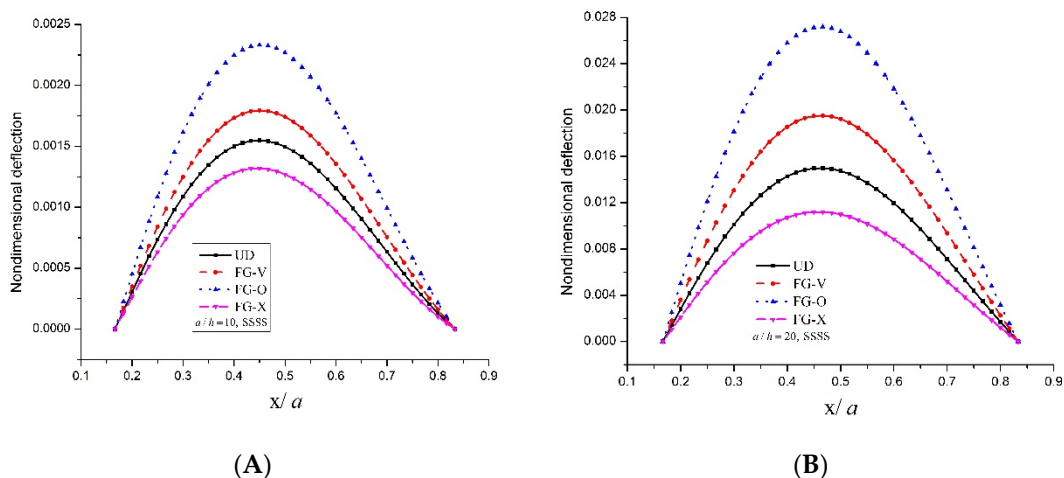


Figure 8. Cont.

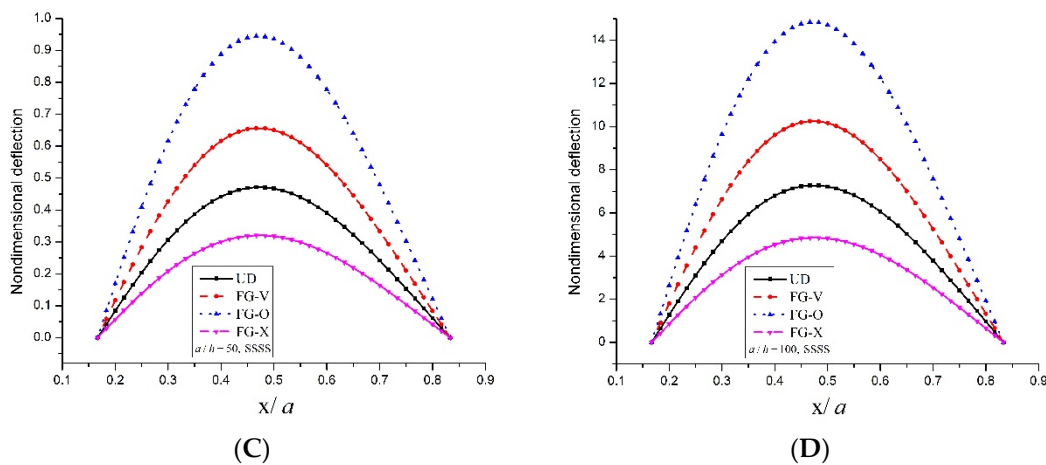


Figure 8. Non-dimensional deflection of FG-CNTRC skew plate along the length ($y/b = 0.5$) subjected to sin-sin loading for (A) $a/h = 10$; (B) $a/h = 20$; (C) $a/h = 50$ and (D) $a/h = 100$.

Figures 9 and 10 show the variation of non-dimensional axial stress for FG-CNTRC rhombic plate subjected to sin-sin loading for simply supported and clamped boundary condition, respectively. The dimensionless value of axial stress decreases with an increase in the skew angle and same nature of variation in thickness coordinate was noticed for all values of skew angles.

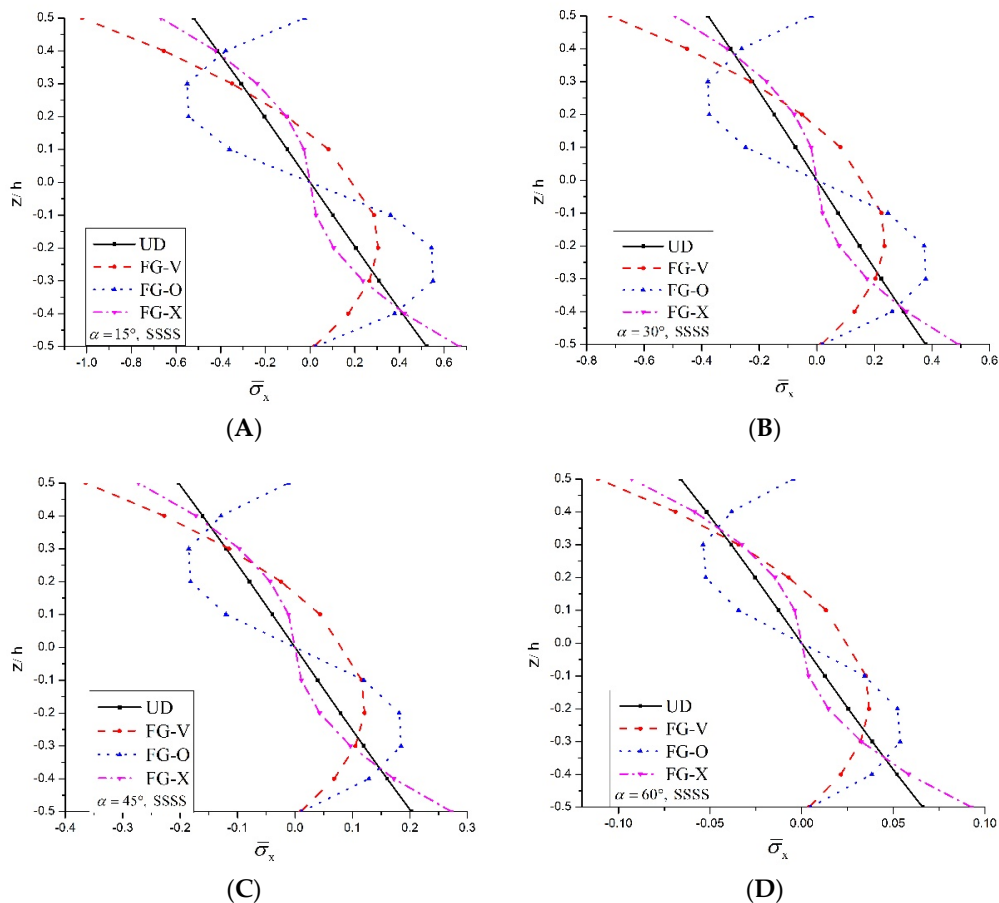


Figure 9. Variation of non-dimensional axial stress for FG-CNT-reinforced rhombic plate subjected to sin-sin loading for (A) $\alpha = 15^\circ$, (B) $\alpha = 30^\circ$, (C) $\alpha = 45^\circ$ and (D) $\alpha = 60^\circ$.

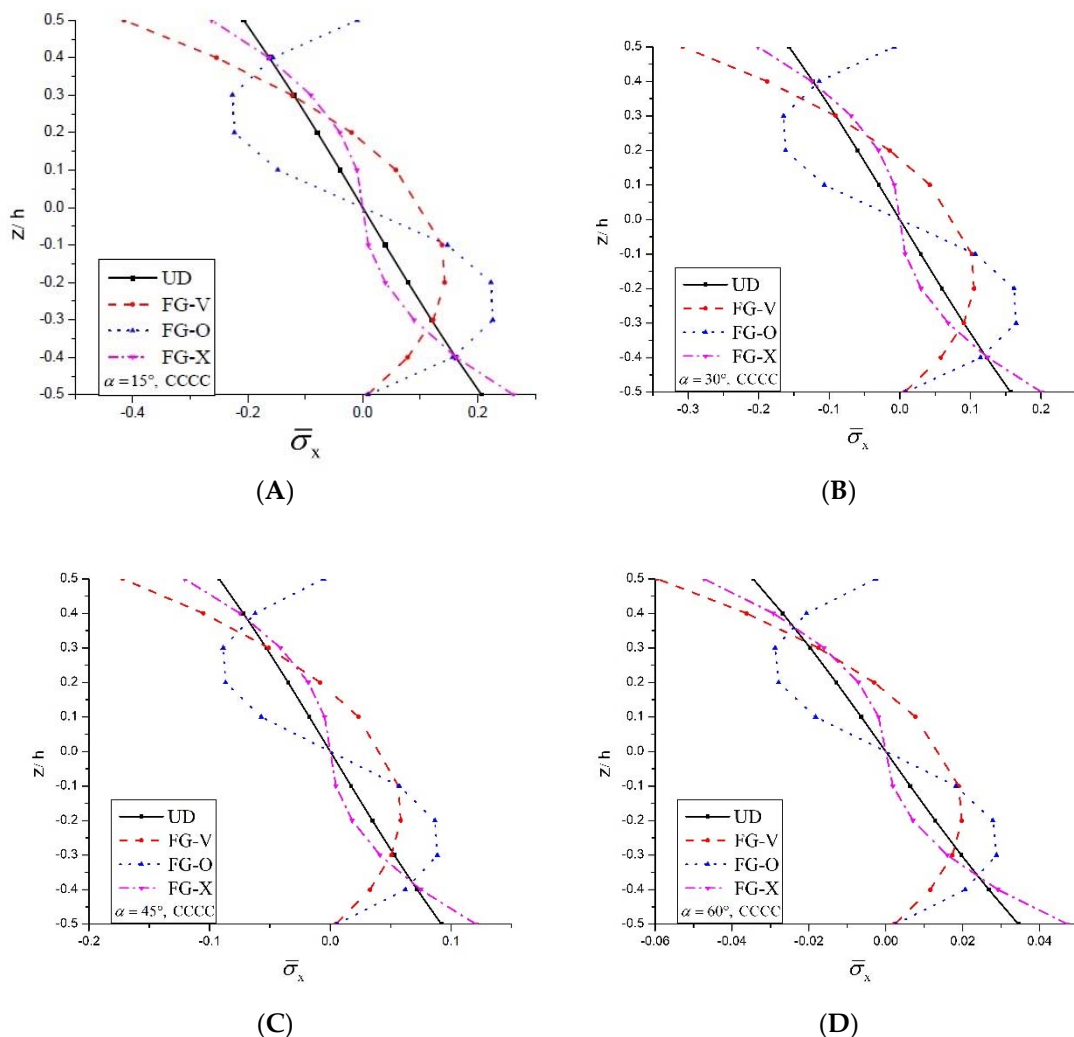


Figure 10. Variation of non-dimensional axial stress for FG-CNT-reinforced rhombic plate subjected to sin-sin loading **(A)** $\alpha = 15^\circ$, **(B)** $\alpha = 30^\circ$, **(C)** $\alpha = 45^\circ$ and **(D)** $\alpha = 60^\circ$.

6. Conclusions

The static and free vibration analyses of FG-CNT-reinforced rhombic plate under various types of load considering various combinations of end support using an efficient C^0 finite element model based on TSDT were presented. The actual material properties at any given section are calculated using the rule of mixture. The following conclusions written below were drawn from the obtained results for numerous values of side-to-thickness ratio, skew angle, and aspect ratio, and different types of end support.

- The FG-O and FG-X type distributions inside the CNT rhombic plates have lower and higher non-dimensional frequency parameter as well as higher and lower dimensionless deflection, respectively.
- The rise in the CNTs volume fraction results in a decrease in the deflection and an increase in the frequency parameter of the CNT-reinforced rhombic plate.
- The dimensionless frequency parameter increases along with the skew angle, irrespective of the CNT distribution and boundary condition.
- Maximum dimensionless deflection and dimensionless normal stresses decrease along with the skew angle.

- Higher values of non-dimensional fundamental frequencies and lower values of dimensionless deflection are found for greater constraints on boundaries.

Author Contributions: M.I.A. and A.K. conceived the idea of the experiment, conducted the experiments, and analyzed the results. M.I.A., A.K., D.B.-H. and Z.S. analyzed the results and discussed the experimental results. W.A. provided manuscript formatting, Z.S.: language correction. All authors provided substantive comments.

Acknowledgments: The authors are thankful for the Financial Sanction of the research project FILE No. EMR/2016/004682 by SCIENCE & ENGINEERING RESEARCH BOARD (SERB) (a statutory body of the Department of Science & Technology, Government of India). This work was financially supported by Ministry of Science and Higher Education, within the statutory research number S/14/2017 and by the Asia Pro Eco Programme of the European Commission—ASIE/2006/122-432—WASTESAFE II.

Conflicts of Interest: The authors declare no conflict of interest.

Appendix A

Appendix A.1. Element Stiffness Matrix

The derivation of element stiffness matrix for the static and free vibration analysis was presented in this section. By employing the principle of minimum potential energy, the element stiffness matrix can be written as follows:

$$\begin{aligned}[k] &= \sum_{i=1}^{nu+nl} \iiint [B]^T [H]^T [\bar{Q}] [H] [B] dx dy dz + [p_0] \\ &= \sum_{i=1}^{nu+nl} \iint [B]^T [D] [B] dx dy + [p_0] \end{aligned},$$

where $[D] = \sum_{k=1}^n \int [H]^T [\bar{Q}] [H] dz$, in which $[B]$ is the strain matrix, $[\bar{Q}]$ is the transformed material constant matrix and $[H]$ is the matrix consisting of the terms containing 'z' and some term related to material properties.

In the abovementioned expression, $[p_0]$ is the penalty matrix added to the stiffness part to compensate for the replacement of the derivatives of transverse displacement ($\partial w / \partial x$ and $\partial w / \partial y$) demanding C^1 continuity by new C^0 continuous variables (w_1 and w_2) following penalty approach, which is a well-known procedure in the finite element analysis. The penalty $[p_0]$ matrix, is expressed as

$$[p_0] = \gamma \iint \left(\left\{ \frac{\partial w}{\partial x} - w_1 \right\}^T \left\{ \frac{\partial w}{\partial x} - w_1 \right\} + \left\{ \frac{\partial w}{\partial y} - w_2 \right\}^T \left\{ \frac{\partial w}{\partial y} - w_2 \right\} \right) dx dy,$$

where γ is the penalty parameter; the value of γ in the present study was assumed as 10^5 .

Appendix A.2. Element Mass Matrix

The consistent mass matrix can be derived in a similar manner to that of the stiffness matrix and was used in the vibration analysis. For the free vibration problem, the acceleration at any point within the plate may be expressed in terms of reference plane parameters:

$$\left\{ \ddot{\bar{f}} \right\} = \frac{\partial^2}{\partial t^2} \left\{ \bar{f} \right\} = \left\{ \begin{array}{c} \ddot{\bar{u}}_0 \\ \ddot{\bar{v}}_0 \\ \ddot{\bar{w}}_0 \end{array} \right\} = -\omega^2 \left\{ \begin{array}{c} \bar{u}_0 \\ \bar{v}_0 \\ \bar{w}_0 \end{array} \right\} = -\omega^2 [F] \{ f \},$$

where the matrix $[F]$ of order 3×7 contains z and some constant quantities like that of $[H]$ and

$$\{ f \} = \left[\begin{array}{ccccccc} u_0 & v_0 & w_0 & \theta_x & \theta_y & \psi_x & \psi_y \end{array} \right]^T.$$

It can finally be expressed in terms of nodal displacement vector $\{\delta\}$, as presented below:

$$\{f\} = [C] \{X\},$$

where $[C]$ is the matrix having an order of 7×63 containing shape functions and its derivatives and $\{X\}$ is the nodal displacement vector containing nodal unknowns for all nine nodes and thus forming a matrix of order 63×1 .

Using the abovementioned equations, the consistent mass matrix of an element can be derived by applying Hamilton's principle and it may be expressed as

$$[m_e] = \sum_{i=1}^{n_u+n_l} \int \rho_i [C]^T [F]^T [F] [C] dx dy dz = \int [C]^T [L] [C] dx dy,$$

where ρ_i is the mass density of the i -th layer and the matrix $[L]$ is

$$[L] = \sum_{i=1}^{n_u+n_l} \int \rho_i [F]^T [F] dz.$$

The stiffness matrix $[K_e]$ (which is 63×63 in the present formulation) and mass matrix $[m_e]$ are computed for all the elements and assembled to form the overall stiffness matrix, $[K]$, and mass matrix, $[M]$, for the total structure. The skyline storage technique is used to keep these large size matrices $[K]$ and $[M]$ in a single array; thus, a considerable amount of storage space in core memory is saved in an efficient manner. This has been implemented systematically in the computer code developed in the present study.

References

- Iijima, S.; Ichihashi, T. Single-shell carbon nanotubes of 1-nm diameter. *Nature* **1993**, *363*, 603–605. [[CrossRef](#)]
- Hone, J.; Llaguno, M.C.; Biercuk, M.J.; Johnson, A.T.; Batlogg, B.; Benes, Z.; Fischer, J.E. Thermal properties of carbon nanotubes and nanotube-based materials. *Appl. Phys. A Mater. Sci. Process.* **2002**, *74*, 339–343. [[CrossRef](#)]
- Dresselhaus, M.S.; Dresselhaus, G.; Charlier, J.C.; Hernandez, E. Electronic, thermal and mechanical properties of carbon nanotubes. *Philos. Trans. R. Soc. A Math. Phys. Eng. Sci.* **2004**, *362*, 2065–2098. [[CrossRef](#)] [[PubMed](#)]
- Reissner, E. On the theory of transverse bending of elastic plates. *Int. J. Solids Struct.* **1976**, *12*, 545–554. [[CrossRef](#)]
- Zhu, P.; Lei, Z.X.; Liew, K.M. Static and free vibration analyses of carbon nanotube-reinforced composite plates using finite element method with first order shear deformation plate theory. *Compos. Struct.* **2012**, *94*, 1450–1460. [[CrossRef](#)]
- Lei, Z.X.; Liew, K.M.; Yu, J.L. Free vibration analysis of functionally graded carbon nanotube-reinforced composite plates using the element-free kp-Ritz method in thermal environment. *Compos. Struct.* **2013**, *106*, 128–138. [[CrossRef](#)]
- Moradi-dastjerdi, R.; Foroutan, M.; Pourasghar, A.; Sotoudeh-bahreini, R. Static analysis of functionally graded carbon nanotube-reinforced composite cylinders by a mesh-free method. *J. Reinf. Plast. Compos.* **2013**, *32*, 593–601. [[CrossRef](#)]
- Yas, M.H.; Pourasghar, A.; Kamarian, S.; Heshmati, M. Three-dimensional free vibration analysis of functionally graded nanocomposite cylindrical panels reinforced by carbon nanotube. *Mater. Des.* **2013**, *49*, 583–590. [[CrossRef](#)]
- Malekzadeh, P.; Zarei, A.R. Free vibration of quadrilateral laminated plates with carbon nanotube reinforced composite layers. *Thin Walled Struct.* **2014**, *82*, 221–232. [[CrossRef](#)]
- Nami, M.R.; Janghorban, M. Thermal buckling analysis of functionally graded rectangular nanoplates based on nonlocal third-order shear deformation theory. *Adv. Compos. Mater.* **2015**, *24*, 439–450. [[CrossRef](#)]

11. Shahrabaki, E.A.; Alibeigloo, A. Three-dimensional free vibration of carbon nanotube-reinforced composite plates with various boundary conditions using Ritz method. *Compos. Struct.* **2014**, *111*, 362–370. [[CrossRef](#)]
12. Sankar, A.; Natarajan, S.; Ganapathi, M. Dynamic instability analysis of sandwich plates with CNT reinforced facesheets. *Compos. Struct.* **2016**, *146*, 187–200. [[CrossRef](#)]
13. Mehar, K.; Panda, S.K. Vibration analysis of functionally graded carbon nanotube reinforced composite plate in thermal environment. *J. Sandw. Struct. Mater.* **2015**, *18*, 151–173. [[CrossRef](#)]
14. Mayandi, K.; Jeyaraj, P. Bending, buckling and free vibration characteristics of FG-CNT polymer composite beam under non-uniform thermal load. *Proc. Inst. Mech. Eng. Part L J. Mater. Des. Appl.* **2015**, *229*, 13–28. [[CrossRef](#)]
15. Zhang, L.W.; Cui, W.C.; Liew, K.M. Vibration analysis of functionally graded carbon nanotube reinforced composite thick plates with elastically restrained edges. *Int. J. Mech. Sci.* **2015**, *103*, 9–21. [[CrossRef](#)]
16. Huang, B.; Guo, Y.; Wang, J.; Du, J.; Qian, Z.; Ma, T.; Yi, L. Bending and free vibration analyses of antisymmetrically laminated carbon nanotube-reinforced functionally graded plates. *J. Compos. Mater.* **2016**, *51*, 3111–3125. [[CrossRef](#)]
17. García-macías, E.; Castro-triguero, R.; Saavedra, E.I.; Friswell, M.I.; Gallego, R. Static and free vibration analysis of functionally graded carbon nanotube reinforced skew plates. *Compos. Struct.* **2016**, *140*, 473–490. [[CrossRef](#)]
18. Mirzaei, M.; Kiani, Y. Free vibration of functionally graded carbon nanotube reinforced composite cylindrical panels. *Compos. Struct.* **2016**, *142*, 45–56. [[CrossRef](#)]
19. Song, Z.G.; Zhang, L.W.; Liew, K.M. Vibration analysis of CNT-reinforced functionally graded composite cylindrical shells in thermal environments. *Int. J. Mech. Sci.* **2016**, *115–116*, 339–347. [[CrossRef](#)]
20. Thomas, B.; Roy, T. Vibration analysis of functionally graded carbon nanotube-reinforced composite shell structures. *Acta Mech.* **2016**, *599*, 581–599. [[CrossRef](#)]
21. Duong, H.M.; Gong, F.; Liu, P.; Tran, T.Q. Advanced Fabrication and Properties of Aligned Carbon Nanotube Composites: Experiments and Modeling. In *Carbon Nanotubes—Current Progress of Their Polymer Composites*; Intech: Houston, TX, USA, 2016; pp. 47–72. ISBN 978-953-51-2470-2.
22. Selim, B.A.; Zhang, L.W.; Liew, K.M. Vibration analysis of CNT reinforced functionally graded composite plates in a thermal environment based on Reddy's higher-order shear deformation theory. *Compos. Struct.* **2016**, *156*, 276–290. [[CrossRef](#)]
23. Zhang, L.W.; Selim, B.A. Vibration analysis of CNT-reinforced thick laminated composite plates based on Reddy's higher-order shear deformation theory. *Compos. Struct.* **2017**, *160*, 689–705. [[CrossRef](#)]
24. Manevitch, L.I.; Smirnov, V.V.; Strozzi, M.; Pellicano, F. Nonlinear optical vibrations of single-walled carbon nanotubes. *Procedia Eng.* **2017**, *199*, 705–710. [[CrossRef](#)]
25. Fantuzzi, N.; Tornabene, F.; Bacciochi, M.; Dimitri, R. Free vibration analysis of arbitrarily shaped Functionally Graded Carbon Nanotube-reinforced plates. *Compos. Part B* **2017**, *115*, 384–408. [[CrossRef](#)]
26. Tornabene, F.; Fantuzzi, N.; Bacciochi, M. Linear static response of nanocomposite plates and shells reinforced by agglomerated carbon nanotubes. *Compos. Part B* **2017**, *115*, 449–476. [[CrossRef](#)]
27. Romano, G.; Barretta, R. Nonlocal elasticity in nanobeams: The stress-driven integral model. *Int. J. Eng. Sci.* **2017**, *115*, 14–27. [[CrossRef](#)]
28. Romano, G.; Barretta, R.; Diaco, M. On nonlocal integral models for elastic nano-beams. *Int. J. Mech. Sci.* **2017**, *131–132*, 490–499. [[CrossRef](#)]
29. Mahmoudpour, E.; Hosseini-Hashemi, S.H.; Faghidian, S.A. Nonlinear vibration analysis of FG nano-beams resting on elastic foundation in thermal environment using stress-driven nonlocal integral model. *Appl. Math. Model.* **2018**, *57*, 302–315. [[CrossRef](#)]
30. Barretta, R.; Ali Faghidian, S.; Luciano, R.; Medaglia, C.M.; Penna, R. Stress-driven two-phase integral elasticity for torsion of nano-beams. *Compos. Part B Eng.* **2018**, *145*, 62–69. [[CrossRef](#)]
31. Oskouie, M.F.; Ansari, R.; Rouhi, H. Bending of Euler-Bernoulli nanobeams based on the strain-driven and stress-driven nonlocal integral models: A numerical approach. *Acta Mech. Sin.* **2018**. [[CrossRef](#)]
32. Barretta, R.; Faghidian, S.A.; Luciano, R. Longitudinal vibrations of nano-rods by stress-driven integral elasticity. *Mech. Adv. Mater. Struct.* **2018**. [[CrossRef](#)]
33. Ansari, R.; Torabi, J.; Shakouri, A.H. Vibration analysis of functionally graded carbon nanotube-reinforced composite elliptical plates using a numerical strategy. *Aerospace Sci. Technol.* **2017**, *60*, 152–161. [[CrossRef](#)]

34. Tornabene, F.; Bacciochi, M.; Fantuzzi, N.; Reddy, J.N. Multiscale Approach for Three-Phase CNT/Polymer/Fiber Laminated Nanocomposite Structures. *Polym. Compos.* **2017**. [[CrossRef](#)]
35. Ardestani, M.M.; Zhang, L.W.; Liew, K.M. Isogeometric analysis of the effect of CNT orientation on the static and vibration behaviors of CNT-reinforced skew composite plates. *Comput. Methods Appl. Mech. Eng.* **2017**, *317*, 341–379. [[CrossRef](#)]
36. Esawi, A.M.K.; Farag, M.M. Carbon nanotube reinforced composites: Potential and current challenges. *Mater. Des.* **2007**, *28*, 2394–2401. [[CrossRef](#)]
37. Fidelus, J.D.; Wiesel, E.; Gajny, F.H.; Schulte, K.; Wagner, H.D. Thermo-mechanical properties of randomly oriented carbon/epoxy nanocomposites. *Compos. Part A Appl. Sci. Manuf.* **2005**, *36*, 1555–1561. [[CrossRef](#)]
38. Shen, H.S. Nonlinear bending of functionally graded carbon nanotube-reinforced composite plates in thermal environments. *Compos. Struct.* **2009**, *91*, 9–19. [[CrossRef](#)]
39. Reddy, J.N. A simple higher-order theory for laminated composite plates. *J. Appl. Mech.* **1984**, *51*, 745–752. [[CrossRef](#)]
40. Han, Y.; Elliott, J. Molecular dynamics simulations of the elastic properties of polymer/carbon nanotube composites. *Comput. Mater. Sci.* **2007**, *39*, 315–323. [[CrossRef](#)]
41. Reddy, J.N. *An Introduction to the Finite Element Method*; McGraw-Hill: New York, NY, USA, 1993.
42. Srinivas, S.; Joga Rao, C.V.; Rao, A.K. An exact analysis for vibration of simply-supported homogeneous and laminated thick rectangular plates. *J. Sound Vib.* **1970**, *12*, 187–199. [[CrossRef](#)]
43. Mantari, J.L.; Oktem, A.S.; Soares, C.G. Bending and free vibration analysis of isotropic and multilayered plates and shells by using a new accurate higher-order shear deformation theory. *Compos. Part B* **2012**, *43*, 3348–3360. [[CrossRef](#)]



© 2018 by the authors. Licensee MDPI, Basel, Switzerland. This article is an open access article distributed under the terms and conditions of the Creative Commons Attribution (CC BY) license (<http://creativecommons.org/licenses/by/4.0/>).